# Distinct neural bases of subcomponents of the attentional blink

**Authors & Affiliations:**

Swagata Halder[1]*, Deepak Velgapuni Raya[1], Devarajan Sridharan[1,2]*

[1]Centre for Neuroscience, Indian Institute of Science, Bangalore, India, and

[2]Computer Science and Automation, Indian Institute of Science, Bangalore, India

***Correspondence to:**

Swagata Halder,
Graduate Program in Neuroscience,
Centre for Neuroscience,
Indian Institute of Science,
C. V. Raman Avenue,
Bangalore 560012, India
E-mail: swagata@iisc.ac.in

Devarajan Sridharan,
Associate Professor and
DST Swarna Jayanti Fellow,
Centre for Neuroscience,
Indian Institute of Science,
C. V. Raman Avenue,
Bangalore 560012, India
Phone: +91 802 293 3434
E-mail: sridhar@iisc.ac.in

## Abstract

The attentional blink reflects a ubiquitous bottleneck with selecting and processing the second of two targets that occur in close temporal proximity. An extensive literature has examined the attention blink as a unitary phenomenon, As a result, which specific component of attention – perceptual sensitivity or choice bias – is compromised during the attentional blink, and their respective neural bases, remains unknown. Here, we address this question with a multialternative task and novel signal detection model, which decouples sensitivity from bias effects. We find that the attentional blink impairs specifically one component of attention – sensitivity – while leaving the other component – bias – unaffected. Distinct neural markers of the attentional blink mapped on to distinct subcomponents of the sensitivity deficits. Parieto-occipital N2p and P3 potential amplitudes characterized target detection deficits whereas long-range high-beta band (20-30 Hz) coherence between frontoparietal electrodes signalled target discrimination deficits. We synthesized these results with representational geometry analysis. The analysis revealed that detection and discrimination deficits were encoded along separable neural dimensions, whose configural distances robustly correlated with the neural markers of each. Overall, these findings shed new light on subcomponents of the attentional blink, and reveal dissociable neural bases underlying its detection and discrimination bottlenecks.


## Lay summary

In daily life, our attention switches rapidly between different objects. For example, when driving, we may shift focus from a billboard on the roadside to a pedestrian in front, in quick succession. Yet, our ability to process the second object is severely compromised especially when it appears soon after the first: an impairment called the “attentional blink”. In previous work, the attentional blink has been studied essentially as a “monolithic” (indivisible) phenomenon. We design a behavioral model to divide the attentional blink into sub-

components and show that the blink affects only one specific component (sensitivity). We also identify key neural markers for deficits associated with this component. Our findings may aid in understanding the neural origins of attention deficit disorders.

## Keywords

attentional deficit; signal detection theory; sensitivity and bias; event-related potentials; long-range synchronization; neural population geometry

## Introduction

Attention is a remarkable cognitive capacity that enables us to process relevant information and filter out irrelevant information to guide Behavior. Yet, attention is surprisingly capacity limited[1]. This limitation is clearly revealed when we seek to perform multiple tasks simultaneously or to tackle multiple goals in rapid succession[2]. A prime example of this capacity limitation is the phenomenon of the attentional blink. When multiple targets are presented sequentially – in a rapid serial visual stream – individuals are often unable to accurately detect and identify the second of two targets, particularly when it is presented in close temporal proximity (200-500 ms) to the first[3] (Fig. 1, left). The inability to process the second target has been hypothesized to arise from various factors, including an inherent delay in reallocating attention from the first target (T1) to the second target (T2)[4,5], a transient bottleneck in working memory while processing the first target[6–10], or an inevitable consequence of suppressing distractors that follow the first target in the visual stream[11–13].

The effect of the attentional blink on the processing of the second target is well studied. In particular, previous studies have investigated the stage at which attentional blink affects T2's processing (early or late) [14–17] and the neural basis of this effect, including the specific brain regions involved[15,18–20]. There is little support for attentional blink deficits at an early, sensory encoding[14] stage; by contrast, the vast majority of literature suggests that T2's processing is affected at a late stage[8,10]. Consistent with these behavioral results, scalp electroencephalography (EEG) studies have reported partial or complete suppression of late event-related potential (ERP) components, particularly those linked to attentional engagement (P2, N2 or N2pc)[15,21,22] or working memory (P3)[20,23,24]; early sensory components (P1/N1) are virtually unaffected[20,22]. These "late" effects are hypothesized to be mediated by diverse functional regions within a frontoparietal network, both based on correlational and causal evidence[25–27]. Activity in the parietal, lateral prefrontal cortex and anterior cingulate cortex, as measured with functional MRI (fMRI) was shown to decrease when T2 was not detected

(missed), even though stimulus-evoked activity in early visual areas (e.g., V1) was relatively intact[28]. Long-range synchronization of EEG oscillations across fronto-parietal regions in the beta-band (13-18 Hz) is impaired during the attentional blink[29]. In addition, converging evidence from transcranial magnetic stimulation (TMS) studies suggest a potentially role for the posterior parietal cortex in the attentional blink[26,27]: T2 detection and identification performance were enhanced after the application of transcranial magnetic stimulation (TMS) over the bilateral parietal cortex.

Despite this extensive literature, previous studies have essentially treated the attentional blink as a unitary, monolithic phenomenon. As a result, fundamental questions regarding the component mechanisms of the attentional blink remain unanswered.

One key question concerns the precise nature of the “late” attentional blink bottleneck. The attentional blink effect is typically quantified as a decrease in the proportion of correct T2 responses at short, relative to long, inter-target lags[3]. Yet, such an impairment can arise from one of at least two processes – a reduction in the fidelity of T2's perceptual representation, a deficit in decision-making based on T2’s representation, or both. Signal detection theory[30] is a widely applied psychophysical framework whose parameters – sensitivity (d’) and bias (or criterion, c) – quantify these perceptual and decisional components, respectively. Distinguishing between sensitivity and criterion effects is crucial because a change in either of these parameters can produce a change in the proportion of correct responses[31,32]. For instance, a lower proportion of correct T2 detections can arise from a lower detection d’, a lower detection bias (higher criterion), or both (Fig. 1, right, top).

Yet, whether the attentional blink induces primarily d’ deficits, primarily bias deficits, or a mixture of both, is largely unknown, and the limited evidence available is controversial[22,33]. This is perhaps because previous studies typically employed simple target detection or identification tasks, in conjunction with conventional, one-dimensional signal detection models[22,33], recent literature suggest that such tasks and models do not suffice to reliably

distinguish between sensitivity and bias components of attention[34–36]. A complete understanding of the attentional blink requires dissociating sensitivity from bias deficits, with appropriate signal detection models, and identifying their respective neural correlates.

A second question concerns the precise nature of attentional blink deficits. Is the attentional blink a deficit with detecting T2 (Fig. 1, right, top) or discriminating T2's features, or both (Fig. 1, right, bottom)? It is evident, from first principles, that distinct neural computations and regions must mediate target detection versus discrimination. For example, detecting a oriented grating in noise can be achieved with a simple, local visual cortex computation: first, by aggregating responses of orientation-tuned visual neurons and then, by testing if this activity exceeds a pre-set threshold[37]. By contrast, discriminating the orientation of a target grating involves an arguably more nuanced computation; one that requires comparing the relative activities of neurons tuned to different orientations relative to some predefined axis (e.g., vertical meridian)[37]. This latter computation would also involve higher cortical areas for maintaining the feature discrimination rule in working memory, such as the prefrontal cortex[38–40]. Moreover, each of these computations could be affected by attention differently[41].

Nonetheless, conventional attentional blink tasks often conflate these computations. In a typical attentional blink task, participants must make identification judgments on T2[3,6]. For example, participants may be asked to identify T2 based on its shape (e.g., a specific letter among numbers) or its category (e.g., a face among non-faces). Yet, an identification deficit during the attentional blink could arise from at least one of two sources[3,4,9,21,29] First, the blink could produce a detection deficit, when the participant fails to reliably detect the occurrence of T2 (Fig 1, Top Right). Alternatively, the blink could produce a discrimination deficit, when the participant detects T2, but is unable to reliably discriminate its features (Fig 1, Bottom Right). A combination of both of these deficits is also possible. To determine the precise

neural underpinnings of the attentional blink deficits, these two deficits must be dissociated, and their respective neural correlates identified.

To tease apart these distinct subcomponents of the attentional blink, we developed a multialternative task that involved concurrent detection of T2 and discrimination of its features (Fig. 2A). To analyze multialternative behavioural responses, we developed a novel two-dimensional signal detection model that decoupled, and separately quantified sensitivity and bias deficits during the blink. With concurrent EEG recordings we analyzed key neural markers – a local neural marker (event-related potentials) potentials and a global marker (oscillatory frontoparietal synchronization) – to test if these would map onto distinct subcomponents of the attention blink (detection and discrimination deficits, respectively). We synthesize these results with representational geometry analysis to understand the neural representations underlying subcomponents of attentional blink-induced deficits. Our results reveal a double dissociation between the neural and behavioral bases of detection and discrimination bottlenecks underlying the attentional blink.

# Results

**The attentional blink produces both detection and discrimination deficits**

Participants (n=24) performed an attentional blink task involving target detection and orientation discrimination (Fig. 2A, see also Methods). In a stream of serially flashed stimuli (100 ms each), the first target (T1) was an oriented grating (radius: 2 dva) of low spatial frequency (0.6 cpd), whereas the second target (T2) was either an oriented grating of comparatively higher spatial frequency (1.8 cpd, 67% of trials) or a blank (33 % of trials). T2 stimuli of high contrast (100%) and low contrast (titrated to individual threshold, see Methods) were interleaved with equal (50%) probability across trials. Targets were interspersed with plaid distractors, and inter-target onset intervals (T1-T2 “lag”-s) were drawn from a geometric distribution (100 ms to 900 ms; see Methods).

Unlike conventional attentional blink tasks[3,6,20], a key element of novelty in our task design was the following: for T1 participants provided a 2-alternative orientation judgement whereas for T2 they provided a 3-alternative, concurrent detection and identification judgement (Fig. 2A). Specifically, at the end of each trial participants first, indicated whether they perceived T1’s orientation to be closer to the cardinal (0°, ±90°) or the diagonal axes (±45°) with two distinct button-press responses (two-alternative forced choice or 2-AFC) (Fig. 2A, penultimate panel from the right). Then, participants reported whether they had detected T2, and if so, whether its orientation was clockwise or counterclockwise of vertical, using 3 distinct button-press responses (three-alternative forced choice or 3-AFC) (Fig. 2A, rightmost). The 3-AFC decision enabled us to decouple the effect of the attentional blink on detection and discrimination performance.

First, we estimated detection and discrimination accuracies for T2 judgements across different T1-T2 lags; these analyses were performed only on trials in which participants provided accurate T1 responses (denoted as “T2|T1” in the figures). Detection accuracies were computed including both the proportions of hits and correct rejections, whereas

discrimination accuracies were computed based on the proportion of correct identifications (Methods). T2 detection accuracies were markedly lower at the short (100 ms and 300 ms), as compared to the long, inter-target lags (700 and 900 ms) (Fig. 2B); this induced a significant detection deficit, measured as the difference in detection accuracies between the short and the long lags (detection deficit = -8.9 ± 1.6%, mean ± s.e.m., $p<0.001$, Wilcoxon signed rank test, $BF>10^2$; data pooled across T2 contrasts). Similarly, T2 discrimination accuracies were also significantly lower at the short lags compared to the long lags (discrimination deficit = -13.5 ± 1.8%, $p <0.001$, $BF>10^2$) (Fig. 2C). In other words, the attentional blink induced both a significant detection and a discrimination deficit for the processing of the second target.

Next, we tested if the magnitude of either the detection or the discrimination deficit would vary depending on T2 stimulus contrast. For this we performed a two-way ANOVA with either the detection or the discrimination accuracy as the response variable and lags (short or long) and contrast (high/HC or low/LC) as independent factors. While we found a main effect of both lag (detection: $F(1,23)=29.8$, $p<0.001$, discrimination: $F(1,23)=54.1$, $p<0.001$) and contrast (detection: $F(1,23)=21.02$, $p<0.001$, discrimination: $F(1,23) =13.75$, $p=0.001$), we found no significant interaction effect between lag and contrast (detection: $F(1,23)=1.92$, $p=0.113$, discrimination: $F(1,23) = 0.93$, $p=0.450$). In other words, attentional blink-induced both a detection and discrimination deficit regardless of stimulus contrast.

Finally, rather than analyzing deficits with overall accuracies, we also analyzed blink-induced effects on individual behavioral responses in the 3x3 stimulus-response contingency table for the 3-AFC task (Fig. 2D). These responses fall under five categories – hits, correct rejections, misidentifications, false alarms, and misses (Methods). Again, a two-way ANOVA revealed a main effect of inter-target lag for all five response types ($p<0.01$; SI Table S1): essentially all correct response proportions (hits, correct rejections) decreased, and incorrect response proportions (false alarms, misses and misidentifications) increased, at short relative to long inter-target lags. A main effect of T2 contrast was observed for hit and miss proportions

(p<0.01) but not for misidentification proportions (p=0.103) (SI Table S1); note that, by definition, false alarms and correct rejection proportions are independent of T2 contrast.

Overall, the attentional blink affected both components of identification – detection and discrimination – in terms of overall accuracy and individual psychometric measures. Whereas detection and discrimination accuracies varied with T2 stimuli's contrast, the strengths of detection and discrimination deficits induced by the blink did not depend on contrast.

**Attentional blink selectively impairs sensitivity, but not the bias, subcomponent.**

While the attentional blink induced deficits with both T2 detection and discrimination, such deficits could arise from either sensitivity or bias/criterion mechanisms. These two possibilities are illustrated in Figure 1, using a one-dimensional, signal detection theory (1-D SDT) model. In the first case (Fig. 1, right, top, upper row), a deficit in T2 detection occurs because of a deterioration in T2's signal evidence strength, which manifests behaviorally as lower perceptual sensitivity. In the second case (Fig. 1, right, top, lower row), the detection deficit occurs because of a more conservative evidence threshold for reporting the presence of T2, which manifests, behaviorally, as a higher criterion, or a lower bias. Either (or both) of these effects could induce an accuracy deficit (Fig.1, left). Similarly, discrimination deficits can occur either because of impaired sensitivity (Fig. 1, right, bottom, upper row) or a sub-optimal bias (Fig. 1, right, bottom, lower row). We sought to distinguish the precise source – sensitivity versus bias – of deficits induced by the attentional blink.

To address this question we developed a novel, two-dimensional signal detection model to analyze participants' T2 judgments in the 3-AFC task (see Discussion). Note that such multialternative responses cannot be correctly analyzed with a combination of one-dimensional SDT models; the reasons are discussed in detail in previous studies[32,42] (see also Discussion). Briefly, the three-alternative decision is modeled in a 2-dimensional decision space: evidence for the presence (or absence) of T2 represented along the abscissa and evidence for clockwise or counterclockwise orientations for T2 represented along the ordinate

(Fig. 3A); we term these the “detection” (y-axis) and “discrimination” (x-axis) axes, respectively. On each trial, a bivariate decision variable (**ψ**) encodes T2’s features, with **ψ**'s component along the detection and discrimination axes representing evidence for T2’s presence ($\psi_{det}$) and T2’s orientation ($\psi_{dis}$), respectively. The distribution of **ψ**, across trials, is modeled as a bivariate, isotropic Gaussian whose mean varies with T2’s configuration across each of five conditions (Fig. 3A-B; absent, LC/CW, LC/CCW, HC/CW, HC/CCW); thus, the model incorporates one noise distribution (T2 absent), centered at the origin, and four signal distributions. The means of the signal distributions along the detection and discrimination axes represent the participant’s sensitivity for detecting T2 ($d'_{det}$) and discriminating its orientation ($d'_{dis}$), respectively. An inverted-Y shaped decision surface divides the decision space into 3 decision zones, one corresponding to each type of response: T2 clockwise (upper right), T2 counter-clockwise (upper left) or T2 absent (lower). The decision surface is parameterized by a detection threshold ($t_{det}$) and a discrimination criterion ($c_{dis}$); these parameters determine the placement of the decision surface along the detection and discrimination axes, respectively. In addition, the angle between the lower arms of the decision surface (β, Fig. 3B) is estimated as a free parameter of the model. The model was fit to the 3x3 stimulus-response contingency table derived from participants’ 3-AFC responses (Methods) with maximum likelihood estimation.

We fit five variants of the model with different constraints on the parameters based on distinct sets of plausible assumptions: these included constraints on the parameters across lags, as well as across low and high contrast T2 stimuli (Methods; SI Fig. S1A). Model comparison analysis – based both on the Akaike Information Criterion (AIC)[43] and the Bayesian information criterion (BIC)[43] – identified a model in which discrimination sensitivity ($d'_{dis}$) was equal for high and low contrast T2 stimuli for each inter-target lag, and discrimination criterion ($c_{dis}$) and angle (β) were equal across lags (Model III, SI Fig. S1A, C-D). Goodness-of-fit p-values (Methods) were generally high for this model, (median >0.95; SI Fig. S1B) indicating satisfactory model fits to data.

The attentional blink significantly impaired both detection and discrimination sensitivity. T2 detection d' was significantly lower at short, compared to long, inter-target lags ($d'_{det}$ deficit = -0.94 ± 0.17, $p<0.001$, signrank test; $BF>10^3$, data pooled across T2 contrasts) (Fig 3C). Similarly, T2 discrimination d' was also significantly lower at the short lags compared to the long lags ($d'_{dis}$ deficit = -0.61 ± 0.06, $p<0.001$; $BF>10^3$) (Fig 3D). A two-way ANOVA with inter-target lag and T2 contrast as independent factors revealed a main effect of lag on both $d'_{det}$ ($F(1,23)=30.3$, $p<0.001$) and $d'_{dis}$ ($F(1,23)=100.3$, $p<0.001$). Yet, we found no significant interaction effect between lag and contrast for $d'_{det}$ ($F(1,23)=2.3$, $p=0.141$). A similar interaction analysis could not be performed for $d'_{dis}$ as this parameter was constrained to be equal across contrasts, based on model selection analysis.

By contrast, attentional blink produced no systematic effect on either detection or discrimination criteria. Even though the detection threshold ($t_{det}$) was higher at short, compared to long, inter-target lags ($t_{det}$ deficit = -0.59 ± 0.17, $p<0.001$, BF=14), the detection criterion ($c_{det}$) – the conventional SDT measure of bias (Methods) – was not significantly different across lags ($c_{det}$ deficit = -0.16 ± 0.16, $p= 0.775$, BF=0.34) (Fig 3E). Moreover, model selection analysis had already identified a model in which the discrimination criterion ($c_{dis}$) was constrained to be invariant across lags (Fig 3F), obviating analyses of lag effects on this parameter. Nonetheless, estimating this criterion – even with an unconstrained model – revealed no evidence for a significant blink effect ($c_{dis}$ deficit = 0.02 ± 0.04, $p=0.627$, BF=0.23).

Finally, we tested whether detection and discrimination deficits were likely to be mediated by common or dissociable processes. For this, first, we correlated the magnitude of the blink-induced detection and discrimination sensitivity deficits – the d' modulation index (MI) – across participants (Methods). Detection and discrimination d' deficits were only weakly, and non-significantly, correlated ($r=0.39$, $p=0.059$) (SI Fig. S2, left); similar results were obtained upon correlating accuracy deficits also (SI Fig. S2, right). In general, detection d' deficits varied widely even among individuals exhibiting a narrow range of discrimination deficits, and vice versa (SI Fig. S2A-B). Second, we tested whether the strength of detection and discrimination

accuracy deficits would co-vary within each participant. For this, we divided task blocks into those with the highest and lowest detection accuracy MIs and compared the magnitude of the discrimination accuracy MI across these blocks (Methods). The difference in discrimination accuracy deficits across high and low detection accuracy deficit blocks was not significant ($p=0.067$, BF=1.42) (Fig. 3G).

In summary, we developed a novel, two-dimensional signal detection model to simultaneously quantify blink-induced effects on T2's detection and discrimination. The attentional blink affected both detection and discrimination sensitivity, across T2 stimuli of high and low contrasts. Yet, no measurable effect occurred on detection or discrimination criteria. In other words, performance deficits induced by the attentional blink could be attributed entirely to sensitivity, rather than criterion, effects. Moreover, detection and discrimination d' deficits were only weakly, and non-significantly, correlated both within and across participants suggesting potentially distinct neural underpinnings. Next, we investigated electrophysiological correlates of these behavioral deficits.

**Dissociable electrophysiological markers of detection versus discrimination deficits**

We sought to identify electrophysiological correlates of detection and discrimination deficits during the attentional blink. As a first step, we examined the effect of established signatures of the attentional blink, including event-related potential (ERP) magnitude[15,20] and long-range synchronization[29]. EEG data were acquired from a subset (n=18/24) of participants, while they were tested on the behavioral paradigm (Methods); high and low contrast T2 trials were pooled to estimate reliable ERPs (Methods). Because detection and discrimination d' deficits were weakly correlated, we identified specific neural correlates of each by quantifying the partial correlation ($r_p$) between the amplitudes of each EEG metric across lags and either detection d' ($d'_{det}$) or discrimination d' ($d'_{dis}$), while controlling for the value of the other parameter ($d'_{dis}$ or $d'_{det}$, respectively) (Methods).

First, we quantified the change in peak amplitude for different ERP components conventionally associated with the attentional blink: occipital P1[20,22], frontocentral P2[44,45], occipital N2p[20,22,24,45] and parietal P3[45–48] (Figs. 4A-B, left). Among these ERP components, the N2p component and the P2 component were both significantly suppressed during the blink (Δamplitude, short-lag – long-lag: N2p=-0.47 ± 0.12 μV, p=0.003, P2=-0.19 ± 0.07 μV, p=0.021, signed rank test) (Fig. 4A, right). Similarly, the parietal P3 also showed a significant blink-induced suppression (P3= -0.45 ± 0.09μV, p < 0.001) (Fig. 4B, right). By contrast the occipital P1, an early sensory component, did not show significant blink-induced modulation (P1= -0.24 ± 0.11, p=0.050) (SI Fig. S3). Results from various studies support each of these findings[20].

Next, we tested whether distinct ERP components correlated specifically with detection versus the discrimination deficits induced by the attentional blink. Detection d' correlated both with the N2p and P3 amplitudes (Fig. 4C and 4E) (partial correlation, N2p: $r_p$=0.34 p<0.001, P3: $r_p$=0.30, p<0.001, permutation test) (Fig. 4D and 4F, top). However, discrimination d' correlated with neither of these components (N2p: $r_p$=-0.01, p=0.970; P3: $r_p$=0.14, p=0.748) (Fig. 4D-F, bottom). Yet, despite its amplitude being significantly modulated by the blink, the frontocentral P2 component did not correlate with either detection d' ($r_p$=0.05, p=0.999) or discrimination d' ($r_p$=0.23, p=0.120). Similarly, the P1 component did not correlate significantly with either detection or discrimination d' (full set of results in SI Table S2). In other words, two key late ERP components (N2p and P3) correlated with detection d' deficits, but not with discrimination d' deficits, each after controlling for the variance explained by the other variable.

Finally, we tested whether long-range synchronization across the brain correlated specifically with blink-induced detection or discrimination deficits. Following previous reports[23,29] we investigated synchronization in the beta-band (13-30 Hz) between frontal and parietal electrodes using spectral coherence (Methods). We observed a strong and sustained decrease in fronto-parietal coherence during the attentional blink particularly, in the high-beta

(20-30 Hz) band (Fig. 5A-B, $\Delta PLV = PLV_{short\text{-}lag} - PLV_{long\text{-}lag}$). Hemisphere-wise analysis revealed a marked and significant reduction in fronto-parietal high-beta coherence over the left hemisphere, in a cluster from 0 to 300 ms post T2 onset (permutation test, $p=0.038$, corrected; cluster-forming threshold $p<0.05$) (Fig. 5C); by contrast, no discernible effects occurred over the right hemispheric fronto-parietal electrodes ($p>0.05$) (Fig. 5D). Furthermore, we tested whether high-beta coherence varied with detection d' or discrimination d', lag-wise, with partial correlations (Methods). Discrimination d', but not detection d', significantly correlated with left fronto-parietal coherence in the high-beta band ($d'_{dis}$: $r_p=0.22$, $p=0.018$; $d'_{det}$: $r_p=-0.05$, $p=0.316$) (Fig. 5E-F).

We also examined correlations between detection d' or discrimination d' and low-beta (13-19 Hz) coherence, as well as with beta coherence over right hemispheric fronto-parietal electrodes but found no significant results; the full set of correlations is shown in SI Table 3.

To summarize, we observed a remarkable double dissociation between electrophysiological markers of detection and discrimination deficits induced by the attentional blink: whereas N2p and P3 suppression signaled blink-induced detection d' deficits, reduction in high-beta phase synchronization between left fronto-parietal electrodes signaled discrimination d' deficits.

**Detection and discrimination deficits map to distinct neural dimensions**

Recent studies suggest that an analysis of neural population geometry may provide mechanistic insights into diverse cognitive phenomena[49,50]. Inspired by these findings, we tested whether behavioral detection and discrimination deficits could be mapped to distinct neural dimensions. For this, we quantified the pairwise Euclidean distance, between the centroids of multivariate activity patterns produced by each class of T2 stimuli (clockwise, counterclockwise or no grating) in the posterior electrodes, separately for each inter-target lag (Methods). With these distances, we identified i) a "detection" dimension ($\eta_{det}$), a neural dimension that encoded the presence versus absence of T2 and ii) a "discrimination"

dimension, ($\eta_{dis}$) encoded T2's orientation (clockwise versus counterclockwise) (Methods) (Figs. 6A-B, left). Neural inter-class distances ($||\eta||$) along both the detection and discrimination dimensions decreased significantly during the blink (short lag-long lag: $\Delta||\eta_{det}||$ = -1.30 ± 0.70, p=0.006; $\Delta||\eta_{dis}||$ = -1.23 ± 0.42 p<0.001) (Figs. 6C-D). In other words, neural representations encoding the presence of the target, as well as those encoding the target's features, became more overlapping – or less differentiated – during the attentional blink.

We tested whether the blink-induced collapse along the detection and discrimination neural dimensions would have distinct consequences for behavior. Neural inter-class distance along the detection dimension, $||\eta_{det}||$, revealed a significant partial correlation with detection d' across lags ($r_p$=0.27, p=0.018), but was not correlated with discrimination d' ($r_p$=0.16; p=0.122) (Fig. 6E-F). Conversely, neural inter-class distance along the discrimination dimension, $||\eta_{dis}||$, was significantly correlated with discrimination sensitivity ($r_p$=0.42, p<0.001) but not with detection sensitivity ($r_p$=0.20, p=0.122) (Fig. 6G-H). These results suggest a clear, double dissociation between the neural dimensions that underlie the detection and discrimination deficits induced by the attentional blink.

Next, we tested if inter-class distances along the detection and discrimination dimensions correlated with the magnitude of blink-associated ERPs – the N2p or the P3. The amplitude of the occipital N2p and parietal P3 were both significantly correlated with detection distance, $||\eta_{det}||$ (N2p: $r_p$=0.31, p=0.020; P3: $r_p$=0.46, p<0.001) (Fig. 7A-B and SI Fig. S4A-B), but not with discrimination distance, $||\eta_{dis}||$ (N2p: $r_p$=0.07, p=0.330; P3: $r_p$=0.15, p=0.160). These results further confirm that the N2p and P3 ERP components indicate detection, but not discrimination, bottlenecks underlying the attentional blink.

Finally, we tested whether long-range synchronization between fronto-parietal cortex also varied with distances along these neural dimensions. In particular, we tested if left fronto-parietal coherence correlated with distances along either the detection or the discrimination neural dimension ($\eta_{det}$ or $\eta_{dis}$, respectively). In line with our earlier findings, left frontoparietal

coherence in the high-beta band correlated significantly and specifically with discrimination distance, $||\eta_{dis}||$ ($r_p$=0.26, p=0.039) (Fig. 7C-D), but not with detection distance, $||\eta_{det}||$ ($r_p$=0.07, p=0.255). No such correlation occurred for either right frontoparietal coherence, or for coherence in the low-beta band (SI Table S4). In other words, left hemispheric fronto-parietal synchronization in the high-beta band provides a key marker for the discrimination, but not detection, bottleneck underlying the attentional blink.

Taken together, these results indicate that the attentional blink impaired sensitivity both for detecting T2 and discriminating its features, leaving criteria unaffected. Yet, neural markers signaling detection and discrimination deficits were distinct. Detection deficits were signaled by ERP components such as the occipitoparietal N2p and the parietal P3. On the other hand, discrimination deficits were signaled by long-range high-beta synchronization between left hemispheric frontal and parietal cortex. Additionally, distinct neural dimensions ($\eta_{\mathbf{det}}$ and $\eta_{\mathbf{dis}}$) evidenced representational collapse associated with detection and discrimination deficits and correlated systematically with neural markers of each type of deficit (ERPs, and beta coherence, respectively). These results reveal a clear dissociation between the behavioral and neural bases of detection and discrimination bottlenecks underlying the attentional blink.

## Discussion

When two successive targets appear in close temporal proximity, behavioral judgments about the second target are compromised: a phenomenon termed the attentional blink[3]. We show that attentional blink induces dissociable bottlenecks with both detecting the second target and discriminating its features. Each of these bottlenecks affects the fidelity of the second target's perceptual representations, but do not affect downstream criteria for decisions. Moreover, these bottlenecks map on to distinct neural markers, indicating putatively dissociable mechanisms mediating detection and discrimination deficits.

A significant body of previous work has reported dissociable behavioral and neural mechanisms underlying attention's effects on target detection versus discrimination. Behavioral studies have reported distinct effects on target detection versus discrimination in both endogenous[51] and exogenous[52] attention tasks. Neurally, improved detection of attended targets is accompanied by enhanced neuronal firing[53] or higher ERP amplitudes[54]. On the other hand, improved discrimination of target features may be achieved by selectively facilitating the activity of feature selective neurons[55], especially those that carry maximally discriminative information about the target's features[56]. In addition, attention-induced decorrelation of neuronal firing is hypothesized to systematically aid stimulus discriminability[57], especially under conditions in which signal correlations are high among pairs of neurons[58]. Furthermore, cortical network states become more distinct across object representations, potentially facilitating target discrimination, in endogenous attention tasks[59]. Hence, there was no reason to expect, *a priori,* that impairments induced by the attentional blink on target detection and discrimination would be correlated.

In line with this hypothesis, we discovered that the attentional blink induced dissociable detection and discrimination deficits. There was no evidence for significant association between these two types of deficits within participants, and only a weak correlation of these deficits across participants. Unlike previous target identification designs that heavily conflated

attentional blink's effect on detection versus discrimination performance [3,4,9,21,29], our 3-AFC task, and associated signal detection model enabled quantifying each of these deficits separately, and identifying a double dissociation in their respective neural correlates. The occipital N2p and parietal P3 amplitudes were modulated strongly by the attentional blink and correlated systematically and selectively with detection deficits. Conversely, left hemispheric fronto-parietal high-beta coherence was, again, modulated significantly by the attentional blink and strongly predictive, specifically, of discrimination deficits. By contrast, neither the early occipital P1 nor the frontocentral P2 systematically varied with either detection or discrimination deficits, although the latter ERP was significantly diminished during the attentional blink.

These results extend, and further advance, a significant literature on the attentional blink effects on ERPs[18,20–23,45–47,60–62]. Several previous studies have shown that the occipital N2 component exhibits a higher amplitude on short lag trials in which T2 was successfully detected, versus not[20,22,23,45]. Other studies have shown that the attentional blink also affects the amplitude of N2pc, a posterior, contralateralized N2 component[47,61,63]; a decrease in the amplitude of the N2pc has been hypothesized to index impaired attentional gating of T2. Similarly, previous studies have shown either partial or complete suppression of P2 during the attentional blink.[21,45,61] Yet, these studies reported no change in P2 amplitude between successfully and unsuccessfully detected targets, in line with our own findings. Taken together with our own findings, these results establish the N2 as key marker for successful detection of T2, achieved by robust attentional gating and filtering out of irrelevant temporal (plaid) distractors.

The effect of the attentional blink on the P3 component has been consistently observed in many studies, and its functional significance has been thoroughly investigated. Many studies have reported a systematic reduction in P3 amplitude and latency in both detection and identification tasks, consistent with our own findings[15,20,22,23,46,61,63]. For centrally presented

stimuli, the P3 recorded over parietal cortex is generally linked to high-level cognitive functions, such as consolidation into working memory[64]. In the present study, we observed a selective correlation of the parietal P3 amplitude with detection, rather than discrimination deficits. This suggests that the P3 deficit indexes a specific bottleneck with encoding and consolidating T2 into working memory, rather than an inability to reliably maintain its features.

In contrast to the detection deficits associated with ERP amplitude suppression, discrimination deficits were clearly correlated with disrupted high beta coherence in the frontoparietal electrodes. Although previous studies have shown clear modulations in beta-band coherence during the blink epoch[24,29], the tasks employed in these studies (e.g., letter identification) could not distinguish between detection and discrimination deficits. To our knowledge, ours is the first study to show that modulation of frontoparietal beta synchrony correlates specifically with deficits associated with discrimination performance. This finding is in line with previous literature, which suggests that frontoparietal beta synchrony plays a key role in visual categorization, a function that relies critically on object feature analysis[65]. Beta-band synchrony between the PFC and PPC may carry information about task relevant categories[66]: mechanistically, the oscillations may serve to selectively communicate task relevant features between PFC and PPC[66]. As a result, impairments in beta synchrony may hinder the selection of relevant features leading to a selective discrimination deficit but not detection deficit, as observed in our task. Moreover, previous studies have reported a disruption in beta-band coherence between the left frontal and right parietal cortex[24,67]. Yet, we observed significant left lateralization of frontoparietal beta-band coherence during the attentional blink (Fig. 5B). One possibility is that this lateralization arises from beta oscillations in the left motor cortex signaling right-handed responses[68]. We discount this hypothesis for multiple reasons. First, the left-lateralization of the high-beta coherence occurred closely following T2 onset, many hundreds of milliseconds before the response epoch. Second, the beta coherence deficit correlated specifically with only one kind of perceptual deficit (discrimination, but not detection). Finally, in our tasks, participants reported T2's orientation

with a bimanual response – the left index finger to report clockwise orientations and the right index finger to report counter-clockwise orientations. In other words, motor-activity linked beta oscillations were highly unlikely to be the source of the lateralized coherence deficits observed in our study.

Both successful target detection and discrimination improve significantly with stimulus contrast.[69] We had, therefore, expected to observe stronger detection and discrimination d' deficits for low contrast, as compared to high contrast targets. Surprisingly, we found no significant effect of contrast on either type of deficit (Figs. 2A-B). In other words, high (100%) contrast T2 stimuli were also strongly susceptible to the detection and discrimination bottlenecks associated with the attentional blink. Thus, despite a clear contrast-dependent encoding of T2 in early sensory cortex, the attentional blink resulted in a significant deficit with its subsequent downstream processing that occurred even for targets of high contrast. These results confirm a late processing bottleneck, consistent with findings from several previous studies[3,20,70]

But what specific neural computation underlies this late bottleneck? Previous research has documented three key computational stages mediating perceptual decisions: encoding of sensory evidence, formation of a decision variable, and application of a decision rule when formulating the choice[71]. Our results indicate that the attentional blink impacts, specifically, the second stage, associated with transforming T2's sensory evidence into a decision variable. In fact, our results indicate that the attentional blink did not affect the final, decisional stage, at all: criteria, for both detection and discrimination judgments, were essentially identical across inter-target lags.

These results appear at odds with earlier work, suggesting that the attentional blink produced both sensitivity and criterion effects in a detection task[22,33]. Lasaponara et al[22] reported a decrease in detection bias (likelihood ratio, or LR bias) with lag, whereas Caetta et al.[33] reported an increase in detection criterion with lag. Our study, on the other hand, reports

no change in detection criterion with lag. Our results are potentially consistent with those of Lasaponara et al. Given that d' increases with lag, a constant (positive) detection criterion would mathematically yield a decreasing likelihood ratio bias with lag (LR bias = exp (-d' * c)). In other words, a decrease in LR bias with lag could occur simply because of the increase in detection d' without a concomitant change in detection criterion. On the other hand, a major difference between Caetta et al's study[33] and ours is that Caetta et al modeled a fixed (unvarying) detection threshold across inter-target lags, yielding changes in detection criteria; the latter (detection criteria), and not thresholds, are the conventional SDT measure of bias[33]. Their choice of unvarying thresholds was based on the assumption that participants could not predict the inter-lag of the trial in advance when different lags are interleaved across trials, and, therefore, could not adopt different detection thresholds across lags. By contrast, we considered it more reasonable that participants could modulate their detection thresholds across lags, given that decisions about T2 were made at the end of each trial at which time the participant would be well aware of the inter-target lag for that trial. To explore this hypothesis further, we tested various models including these two models: one with a fixed detection threshold and the other with a variable detection threshold across lags. The results clearly supported a model with varying thresholds and confirmed a constant detection criterion (bias) across lags in our data.

Taken together, these results suggest the following, testable schema (SI Fig. S5). First, smaller N2p and P3 amplitudes may reflect deficits in the activation of neural populations involved in gating and consolidating, respectively, the T2 stimulus into working memory. Second, reduced fronto-parietal high-beta coherence may index deficits in a top-down mechanism that enables discriminating T2's features; the latter computation relies on accurate discrimination of clockwise versus counter-clockwise target orientations. Yet, we found no evidence for these two computations being sequential; in fact, the modulation of beta coherence occurred almost immediately after T2 onset, and lasted well afterwards (>400 ms from T2 onset) (Fig. 5A-B) suggesting that an analysis of T2's features proceeded in parallel

with its detection and consolidation. Finally, decisional processes mediating the conversion of neural evidence for target presence, or orientation, into categorical choices remain unaffected. Future research with causal interventions like tACS or TMS could test this mechanistic schema of specific brain regions or oscillatory patterns in mediating distinct aspects of the attentional blink. More generally, these findings contribute to our understanding of the complex interplay between attention and perception and may be relevant for designing rational interventions for neurological disorders that produce attention deficits.

## Materials and Methods

**Participants**

Twenty-four healthy individuals (9 females; age range: 20-28 years) participated in the study. All participants had normal or corrected to normal vision with no known history of neurological disorders. Among these, scalp electroencephalography (EEG) recordings were acquired concurrently with behavior for eighteen participants. Experimental procedures were approved by the Institute Human Ethics Committee, Indian Institute of Science, Bangalore. Participants provided informed, written consent prior to participating in the experiments.

**Behavioral Data Acquisition**

Apparatus and Stimuli. Participants were tested with a typical Attentional Blink (AB task) protocol involving a rapid serial visual presentation (RSVP) stream (frame rate: 10 stimuli per second; 70 ms on, 30 ms off). Stimulus presentation and data acquisition were programmed with Psychtoolbox[72] and MATLAB 2017b MathWorks Inc. (2017), Natick, MA.). Participants were seated with their head resting on a custom chin rest in a dimly lit room, with their eyes positioned 60 cm away from a contrast-calibrated visual display (24" LCD monitor, 100 Hz refresh rate, BenQ Corp.). Responses were recorded with an RB-840 response box (Cedrus Inc). Participants were instructed to maintain gaze fixation at a central dot throughout the experiment and to avoid eye blinking during the stimulus presentation. Fixation, eye blinks and eye movements were monitored monocularly at 1000 Hz, with an infrared-based eye tracker (Eyelink, SR Research).

Task procedure. Each trial commenced with gaze fixation on a central dot (diameter: 0.5° of visual angle/dva, color: yellow) in the middle of a gray (35 cd/m$^2$ maximum luminance) screen. After 500 ms, task-irrelevant distractors – full contrast plaids (diameter: 4 dva) – appeared in the center of the screen in an RSVP stream (100 ms per stimulus). The plaid comprised of two superposed, square wave gratings (spatial frequency: 1.8 cpd) oriented at 45° and 135°

relative to the vertical, displayed within a circular mask (diameter: 4 dva). The phase of the plaid stimuli underwent a 180° phase inversion (full white to full black, and vice versa) across successive frames of the RSVP presentation. Plaids were encircled by a circular placeholder (diameter: 4.1 dva, thickness: 0.1 dva). The fixation dot and the placeholder were present on the screen throughout the trial.

Following a variable interval (300-1300 ms, geometrically distributed) of plaid presentation, the first target stimulus (T1, oriented square-wave grating, spatial frequency: 0.6 cpd) appeared in the RSVP stream (Fig. 1A). Following another variable interval, the second target stimulus (T2, oriented square-wave grating, 1.8 cpd), higher spatial frequency than T1, was presented in the RSVP stream. The interval between T1 and T2 onsets was geometrically distributed, and pseudorandomly selected from one of 5 possible “inter-target” lags (100, 300, 500, 700 or 900 ms); plaids, identical with those described previously, were presented in the interleaving frames. The T2 grating appeared on only two-thirds of the trials (“T2 present” trials). On the remaining third of the trials, randomly interleaved with the T2-present trials, no T2 was presented (“no T2” trials); rather the plaid was replaced with a gray filled circle (0% contrast) inside the circular placeholder. In addition, on 50% of the trials, T2 gratings were presented at full contrast, whereas on the remaining 50% of the trials (randomly interleaved) T2 grating were presented at a contrast staircased for each participant individually (see next). T1 orientations, as well as T2 orientations and contrasts, were proportionately counterbalanced across all inter-target lags. Finally, plaids were presented for a set of six frames (600 ms) and participants were probed for response.

At the end of each trial, participants provided two responses, one for each of T1 and T2, in succession (Fig. 1A). First, participants indicated whether the T1 grating’s orientation was closer to the cardinal (0°, 90°) or to the diagonal (45°, 135°) axes with one of two button presses (2-alternative forced choice/2-AFC, Fig. 1A). Second, participants indicated whether the T2 grating’s orientation was clockwise of vertical (CW), counter-clockwise of vertical (CCW) or if it was not detected at all (None), with one of three distinct button presses (3-AFC, Fig. 1A).

Training and testing. Two behavioral sessions were conducted on two consecutive days. The first session (on Day 1) comprised of training (30 minutes) followed by a staircasing session (~1.5 hours). The training session typically comprised 2-4 blocks of trials with 84 trials each. Only the longest inter-target lags (700 and 900 ms) were included; short-lag trials were excluded both from this, and the subsequent staircasing, sessions based on previous reports, which suggest that practice effects can mitigate the magnitude of the attentional blink at short-lags[73]. At the end of each trial participants received on-screen feedback regarding their success or failure for each target. For this session, T1 and T2 were both presented at full contrast; T1 was presented with a ±2° deviation from cardinal or diagonal orientations, pseudo randomly counterbalanced among the 4 different options, whereas T2 was presented at ±10° deviation from the vertical. Note that smaller (larger) angular deviations render the cardinal/diagonal (CW/CCW) judgement with the T1 (T2) grating easier. Following this, participants performed a second, staircasing session (~400 trials). In this session, T1's angular deviation from the cardinal/diagonal orientations was staircased to achieve 87.5% discrimination accuracy for T1, whereas T2's contrast was concurrently staircased to achieve 75% discrimination accuracy for T2. T1's angular deviation and T2's contrast determined from this session were used for the main experiment on Day 2; while the former angle was used for all T1 trials, the latter contrast was employed in the low-contrast T2 trials alone.

On Day 2, participants were re-familiarized with the task for ~150-200 trials before the main experiment commenced. Before testing, participants were provided with a 30-minute break. The main experiment comprised trials with all 5 inter-target lags (see above) and comprised 3 blocks of 312 trials each (total of 936 trials per participant). No feedback was provided after each trial. Each block was sub-divided into 4 mini-blocks of 78 trials, and participants were provided short breaks (~5 min) after each mini-block. Data from the staircase and training sessions were excluded from subsequent analyses.

Eye-tracking and data exclusion. Throughout each experiment participants' fixation was monitored and gaze position was recorded and stored for offline analysis. Trials in which an eye blink occurred any time before the response period were excluded from the final analyses. In addition, trials in which the gaze positions deviated from the central pedestal ±50 ms before or after the presentation of either the T1 or the T2 gratings (radius: 2 dva from fixation dot) were excluded from further analysis. Following these exclusions, the median trial rejection rate was 2.1% [0.8-3.4%] (median, 95% confidence interval) across participants.

**Behavioral data analysis**

Measuring attentional blink effects on psychometric quantities. We quantified the effect of the attentional blink on behavioral detection and discrimination psychometrics for the T2 grating. All of the analyses were performed including only trials in which participants made correct responses for the T1 judgment. Our 3-alternative task for T2 judgements, and the associated behavioral model (see next), enabled quantifying psychophysical parameters linked to both detection and discrimination within a single task and analysis framework. Participants' 3-AFC responses for the T2 grating were collated into five 3x3 stimulus-response contingency tables, separately for each of the 5 inter-target lags, and each T2 contrast (high, low). The rows of each contingency table represent the three stimulus events (T2 CW, T2 CCW or no T2) and the columns represent the participants' choices among the three alternatives (Fig. 2C). Each table comprises five responses types – i) Hits (H, elements along the main diagonal, except the bottom right) wherein the subject correctly identifies the orientation of T2 as CW or CCW, ii) Misses (M, last column, except the bottom right), wherein the subject reported "no T2" on trials in which T2 was actually presented, iii) False alarms (FA, last row, except the bottom right), wherein incorrectly reported the presence of T2 (as CW or CCW) when no T2 was presented, iv) Correct Rejections (CR, bottom right), wherein the subject accurately reported the absence of T2, and v) Misidentifications (MI, all other entries), wherein the subject incorrectly reported T2's orientation (CW grating as CCW, or vice versa). We quantified the effect of the attentional blink on each of the psychometric measures by comparing their

respective, average values between the short lag (100 and 300 ms) and long lag (700 and 900 ms) trials; this analysis was performed separately for high and low T2 contrast trials.

Measuring attentional blink effects on psychophysical parameters. We estimated psychophysical parameters by fitting the 3-AFC contingency tables, described above, with a novel signal detection theory (SDT) model. Observers' decisions were modeled in a two-dimensional decision space to fit T2 detection and discrimination performance simultaneously; the model was inspired by the recently published m-ADC model[36] widely used for the analysis of multialternative attention tasks.

*i) Signal detection model description:* On each trial, T2 stimulus' features were encoded with a bivariate Gaussian decision variable (**ψ**). The x-axis of this decision space represents evidence for T2's orientation (CW or CCW), whereas the y-axis represents evidence for T2's presence. In other words, a larger signal magnitude along the x-axis (either positive or negative) favors better discrimination whereas a higher signal magnitude along the y-axis favors more reliable detection. The mean of the bivariate decision variable's value along the x-axis and y-axis is parameterized by two perceptual parameters, indexing perceptual discriminability ($\pm d'_{dis}$) for discriminating T2's orientation, and perceptual sensitivity ($d'_{det}$) for detecting T2's presence, respectively. On the T2 absent trials **ψ** is drawn from a distribution centered at the origin ($d'_{dis}= d'_{det}=0$). On T2 present trials, the decision variable **ψ** is drawn from one of 4 distributions (Fig. 3A), depending on T2's contrast (Fig. 3A; high, low) or its orientation (Fig. 3A; CW, CCW).

The participant makes one of 3 choices – T2 CW, T2 CCW or no T2 – based on a Y-shaped decision surface (Fig. 3B) that divides the decision space into 3 zones (red, blue, or gray shaded regions, respectively). This decision surface is parameterized by three decisional parameters: i) a detection criterion ($c_{det}$) that determines the displacement of this surface along the vertical direction (y-axis), ii) a discrimination criterion ($c_{dis}$) that determines the displacement of this surface along the horizontal direction (x-axis) and iii) an angle (β) between

the two arms of the Y (Fig. 3B). The subject's decision on each trial is based on the decision zone into which **ψ** fell on that trial. Note that the proportion of each type of response for each stimulus event type CW, CCW or no T2 in the stimulus-response contingency table can be mapped to the integral of the conditional density of the decision variable within the decision zone for the respective T2 event and response type. These integrals were evaluated numerically (*integral2* function in Matlab).

Parameters (d', c, β) were estimated with a maximum likelihood estimation approach[36]. Typically, parameters were fit for each lag, independently, unless specified otherwise (see next). Goodness of fit was assessed using a randomisation test based on the chi-squared statistic[36]; $p<0.05$ was taken as evidence of significant deviation of model fits from experimental data.

*ii) Model comparison analysis:* We fit observers' response proportions to five models, each with a set of progressively stronger constraints (decreasing model complexity).

<u>Model I.</u> This model was the least constrained and comprised 35 parameters. 20 perceptual parameters $d'_{det}$ and $d'_{dis}$ were estimated individually for five lags and separately for two T2 contrasts. Similarly, 15 decisional parameters $c_{det}$, $c_{dis}$ and β were estimated individually for each of the 5 lags, separately (15 c and β parameters); because the high and low T2 contrasts trials were randomly interleaved within each block, with no apriori information about which type of target contrast would occur, we modeled these decisional parameters as being identical across high and low T2 contrast trials.

<u>Model II.</u> This model was identical to Model I except that β was constrained to be identical across lags (20 d', 10c, 1 β). Therefore, this model comprised 31 parameters.

<u>Model III.</u> This model was identical with Model II, except that additional constraints were imposed on discrimination-related parameters: i) $d'_{dis}$ was constrained to be identical across contrasts and ii) $c_{dis}$ was constrained to be identical across lags. This model comprised 22 parameters.

Model IV. This model was also identical with Model II, except that additional constraints were imposed on detection-related parameters: i) $d'_{det}$ was constrained to be identical across contrasts and ii) $c_{det}$ was constrained to be identical across lags. This model also comprised 22 parameters.

Model V. This model was the most constrained of all and comprised all constraints in Models II-IV. This model comprised 13 parameters.

Formal model comparison was performed with the Akaike Information Criterion (AIC) and Bayesian Information Criterion (BIC)[43]. These scores represent a trade-off between model complexity (the number of model parameters) and goodness-of-fit (based on the log-likelihood function); a lower AIC/BIC score represents a better candidate model[43]. Based on this analysis, the best model was determined to be Model 3 (see Results, section on "*Detection and discrimination deficits reflect sensitivity, rather than criterion, effects*").

*iii) Quantifying the attentional blink effect:* To quantify the effect of the attentional blink on each of the estimated parameters, the average value of the parameter at the shortest two lags (100 and 300 ms, SL) was subtracted from the average value of the parameters at the longest two lags (700 and 900 ms, LL). e.g, attentional blink effect on detection sensitivity was computed as: $\Delta d'_{det} = d'_{det}^{LL} - d'_{det}^{SL}$. This computation was performed for each T2 contrast separately In some cases (Fig. 3G, SI Fig. S2), the deficit was quantified with a modulation index. e.g. MI-$d'_{det} = (d'_{det}^{LL} - d'_{det}^{SL}.)./ (d'_{det}^{LL} + d'_{det}^{SL}.)$ Because, in the best model selected, $c_{dis}$ and β were constrained to be equal across lags no blink effect was calculated for these parameters. Error bars were computed as the standard error of mean across participants.

**EEG data acquisition and preprocessing**

Acquisition. EEG data were recorded with a dense array of scalp electrodes (128 channels, EGI's Geodesic Inc USA), a Net Amps 400 amplifier, and EGI's Net Station software (version 5.2.0.2, Oregon, USA). During acquisition, data were referenced to the Cz electrode, and

stored for offline analyses. The EEG cap contains a few additional electrodes that are placed around the orbits of the eye and enable monitoring an EOG signal. Channel impedances were monitored and maintained at <50 kΩ during the experiment. Data were sampled at 1000 Hz and stored offline for analysis.

Preprocessing. The data were pre-processed with functions from the EEGLAB toolbox (v. 14.0.0), Chronux toolbox (v. 2.12.03) as well as custom scripts developed in Matlab. First, the data were downsampled to 250 Hz by decimation and bandpass filtered between 0.5 to 18 Hz (FIR filter, *designfilt* function in Matlab). Next, a bandstop filter from 9-11 Hz was applied to remove the 10 Hz oscillations evoked by the RSVP presentation. Channel traces were then re-referenced to the average signal across channels. We then epoched the data into trials and applied SCADS (Statistical Control of Artifacts in Dense Array EEG/MEG Studies[74]) to identify bad epochs and artifact contaminated channels based on outlier values of maximal amplitude, standard deviation, and the first derivative with respect to time. Bad channels were linearly interpolated using data from the four nearest neighbour electrodes. Epochs were demeaned based on a baseline computed in fixation time window (250 ms) at the beginning of each the trial and then quadratically detrended.

**EEG data analysis**

Event Related Potential (ERP) analysis. ERP estimation for this attentional blink task followed a procedure outlined in (Sergent et al.,2005)[20]. First trials were sorted based on inter-target lags (100, 300, 500, 700 and 900 ms); the longest two lags (700 and 900 ms) were combined to provide sufficient trials for robust ERP estimation at these lags. Then, EEG traces were time-aligned to either T1 onset or T2 onset and averaged across trials to estimate T1-evoked and T2-evoked ERPs, respectively. Because of the periodic RSVP presentation these ERPs included strong, plaid-evoked responses, which occurred time-locked to both T1 and T2. To remove this contribution, we subtracted ERPs associated with T2-absent trials (correct rejection trials only) from ERPs associated with T2-present trials (as in[15,20]); this subtraction

was performed separately for each inter-target lag. ERP amplitudes were quantified by measuring peak values within specific time windows corresponding to distinct components. For these analyses we selected four ERP components, routinely studied as neural markers in attentional blink tasks: i) P1 component in occipital electrodes (O1, O2, Oz) between 40 to 140 ms post T2 onset[20,22], ii) N2p component in occipitoparietal electrodes (O1, O2, Oz, P3, P4, Pz and surrounding PO electrodes) between 150 to 300 ms post T2 onset[24,46,47,63], iii) P2 component in frontocentral electrodes (C3,C4,Cz,F3,F4,Fz) between 150 to 300 ms post T2 onset[15,61], iv) P3 component in parietal electrodes (P3,P4,Pz) between 300 to 550 ms post T2 onset[15,20,22,24]. We quantified the change in ERP amplitudes during the attentional blink (see Methods section on "Statistical analyses") and also performed partial correlations between the ERP amplitudes and behavioral metrics (see Methods section on "Partial correlations between neural and behavioral metrics").

<u>Analysis of long-range synchronization.</u> We also quantified long-range synchronization between the frontal and parietal cortex, an established neural marker of the attentional blink[24,29]. For this we quantified the averaged spectral coherence between each pairs of electrodes in the frontal (F3, F4, Fz), and parietal (P3, P4, Pz) cortex (9 pairs), respectively. Coherence measures the degree of functional connectivity at different frequencies between two regions and is quantified as the ratio of the squared of the cross spectral density between the signals normalized by the product of the individual signals' auto spectral densities.

$$C_{xy}(f) = \frac{\left|G_{xy}(f)\right|^2}{\left|G_{xx}(f)\right| \cdot \left|G_{yy}(f)\right|}$$

where $G_{xy}(f)$ denotes the cross spectral density between signals x and y whereas $G_{xx}(f)$ and $G_{yy}(f)$ represent their, respective, auto spectral densities. We computed time frequency representations for coherence (a "coherogram") with the *coherencyc* function in the Matlab Chronux (v2.11) toolbox[75] with a time-half bandwidth product of 3 and 5 tapers ($TxW_{½}$=3, K=5). Coherence values were computed in sliding windows of 300 ms duration with a 50 ms stride computed from -200 ms before to +600 ms following T2 onset. Coherence

values were divisively normalized frequency-wise, on a per-trial basis, with coherence computed in a baseline window from 0-300 ms prior to T2 onset. As with the ERPs, to remove the contribution of T1-evoked responses, coherence values at each time point and frequency of the T2-absent (correct rejection) trials were subtracted from the coherence values of the T2-present trials; this subtraction was performed for each inter-target lag separately. To quantify the effect of the attentional blink on the coherogram, we subtracted the coherograms estimated from the short lag trials (100 and 300 ms) from the corresponding coherograms from the long lag trials (700 and 900 ms). Subsequently, we conducted a cluster-based permutation test on this difference coherogram to identify time periods and frequency bands significantly modulated by the attentional blink (cluster forming threshold $p<0.05$). For subsequent, partial correlation analyses of coherence with behavioral metrics and neural distances (see next), we focused on a 300 ms time period (0-300 ms following T2 onset) and high-beta frequency band (20-30 Hz) identified by the cluster-based permutation test (Fig. 5A-C).

Analysis of neural dimensions corresponding to detection and discrimination deficits. To understand how neural representations of the second target (T2) correlated with behavioral deficits associated with the blink, we constructed distinct dimensions associated with the detection and discrimination of T2. For this, mean EEG traces were computed from 33 bilateral occipito-parietal electrodes (Fig. 6C-D) to form a multivariate activity representation (vector) at each point in time. These time-varying vectors were subtracted against activity vectors on T2 absent (correct rejection) trials, at each corresponding timepoint and across corresponding inter-target lags, as before, to remove the contribution of the T1-evoked component.

We define the detection dimension ($\eta_{det}$) as the vector mean of each of the T2-present activity vectors measured relative to T2-absent activity (Fig. 6A); this dimension reflects the change in average EEG representation between T2 present and T2 absent trials. On the other hand, the discrimination dimension ($\eta_{dis}$) represents the vector difference between the two T2-

present activity vectors (Fig. 6B); this dimension reflects the change in EEG representations between the T2 CW and T2 CCW trials. Each of these dimensions were computed separately for each inter-target lag; the magnitude (L2 norm) of each vector ($||\eta_{det}||$, $||\eta_{dis}||$) represents a scalar quantifying the separability (inverse of the overlap) of the neural representations along the detection or discrimination dimensions, for the respective lag. Note that these vector magnitudes are equivalently computed as the Euclidean distance between the endpoints of the mean vector representing each class of stimuli ("inter-class distance", Fig. 6C-D, left). To mitigate biases arising from different numbers of trials across the different lags, we employed bootstrap resampling: for each inter-target lag we randomly sampled a number of trials corresponding to the lag with the minimum trial count with replacement and computed the mean distances across 10 bootstrap estimates. For quantifying the effect of the attentional blink and for correlation analyses, average inter-class neural distances were computed in a window from 300 to 600 ms following T2 onset (Fig. 6C-D, right). These were then plotted for each lag as a proportion of the inter-class distance for the largest lag (900 ms).

<u>Partial correlations between neural and behavioral metrics.</u> To quantify the neural correlates of blink-induced detection and discrimination deficits, we performed bivariate correlations between neural metrics (ERPs, inter-class distances and coherences) and the behavioral d' for both tasks. The data were pooled across all lags and participants, and neural and behavioral metrics were normalized for each participant by dividing each measure (neural or behavioral) by the sum of that (respective) measure across all lags. Because the detection d' and discrimination d' in our task were weakly correlated, we performed partial correlations, rather than Pearson's correlations, to identify the specific neural correlate of each; these are reported as "$r_p$" in the Results. To assess statistical significance of these coefficients, we performed a non-parametric permutation test by shuffling the labels across lags independently for each measure and participant and computing a null distribution over 1000 such random permutations; the p-value reported is the proportion of $r_p$ values in the null distribution that exceeded the partial correlation coefficient observed in the real data. Partial correlations

between neural metrics (e.g., between inter-class distance and coherence, 7C-D) were also computed with a similar procedure. Due to multiple comparisons, all p-values derived from permutation tests in partial correlation were adjusted using the Bonferroni-Holm correction test.

**Statistical analyses**

For assessing the difference between short-lag and long-lag trials on psychometric or psychophysical metrics (hit, miss, miss identification, false alarm and correct rejections, or d' and c) or neural measures (e.g., ERP amplitudes, coherences, neural distances), non-parametric Wilcoxon-signed rank tests were employed (*signrank* function in Matlab). All tests were conducted as two-sided tests, unless otherwise specified. Additionally, we present the Bayes factor (BF), which is a statistical metric comparing the likelihood of the alternative hypothesis to that of the null hypothesis based on the observed data. The Bayes factor was computed using the JASP toolbox, supported by the University of Amsterdam**.** Goodness-of-fit of the model was assessed using a randomization test based on the $\chi^2$-statistic; the procedure is described in detail in previous work[36,76–79]. A small p-value (e.g., $p<0.05$) indicates that the model fit deviated significantly from the observations. Significance testing for the attentional blink effect on sensitivity (d') and criterion (c) parameters was performed with a 2-way ANOVA test (*anovan* function in Matlab). We employed robust (bend) correlations (Robust Correlation Toolbox, v2. for conventional correlation analyses, and the *parcorr* functon in Matlab for partial correlation analyses. Bonferroni-Holm correction tests were employed through the *bonf_holm* function in MATLAB.

**Data and code availability:** Data and custom Matlab code to replicate the experimental findings as well as the computational modeling results are available at the following link: https://osf.io/gpzbe/?view_only=1140e43e0732451da64c7c9beaaea3d7

## Acknowledgments

This research was supported by a Department of Biotechnology-Wellcome Trust India Alliance Intermediate fellowship, DST Swarna-Jayanti fellowship, a Department of Biotechnology-Indian Institute of Science Partnership Program grant, and an India-Trento Program for Advanced Research grant (all to DS).

## Author Contributions

DS conceptualized the study. SH performed the experiments. SH and DR contributed novel analytic tools and analyzed the data. DS wrote the paper with inputs from all authors.

## Declaration of Interest

Devarajan Sridharan is a research consultant at Google.

## References


1. Desimone, R. & Duncan, J. Neural Mechanisms of Selective Visual Attention. *Annu Rev Neurosci* **18**, 193–222 (1995).
2. Kanwisher Nancy.G and Potter. C. Mary. Repetition Blindness: Levels of Processing. *J Exp Psychol* **16**, 30–47 (1990).
3. Raymond, J. E., Shapiro, K. L. & Arnell, K. M. Temporary suppression of visual processing in an RSVP task: an attentional blink? *J Exp Psychol Hum Percept Perform* **18**, 849–60 (1992).
4. Nieuwenstein, M. R., Potter, M. C. & Theeuwes, J. Unmasking the attentional blink. *J Exp Psychol Hum Percept Perform* **35**, 159–169 (2009).
5. Vul, E., Hanus, D. & Kanwisher, N. Delay of selective attention during the attentional blink. *Vision Res* **48**, 1902–1909 (2008).
6. Shapiro, K. L., Raymond, J. E. & Arnell, K. M. Attention to visual pattern information produces the attentional blink in rapid serial visual presentation. *J Exp Psychol Hum Percept Perform* **20**, 357–371 (1994).
7. Shapiro, K. L., Caldwell, J. & Sorensen, R. E. Personal names and the attentional blink: A visual 'cocktail party' effect. *J Exp Psychol Hum Percept Perform* **23**, 504–514 (1997).
8. Martens, S., Wolters, G. & van Raamsdonk, M. Blinks of the mind: Memory effects of attentional processes. *J Exp Psychol Hum Percept Perform* **28**, 1275–1287 (2002).
9. Chun, M. M. & Potter, M. C. A two-stage model for multiple target detection in rapid serial visual presentation. *J Exp Psychol Hum Percept Perform* **21**, 109–127 (1995).
10. Potter, M. C. *et al.* Bidirectional semantic priming in the attentional blink. *Psychon Bull Rev* **12**, 460–465 (2005).
11. Di Lollo, V., Kawahara, J., Shahab Ghorashi, S. M. & Enns, J. T. The attentional blink: Resource depletion or temporary loss of control? *Psychol Res* **69**, 191–200 (2005).
12. Nieuwenstein, M. R. & Potter, M. C. Temporal Limits of Selection and Memory Encoding. *Psychol Sci* **17**, 471–475 (2006).
13. Kawahara, J.-I., Kumada, T. & di Lollo, V. The attentional blink is governed by a temporary loss of control. *Psychon Bull Rev* **13**, 886–890 (2006).
14. Zivony, A., Shanny, S. & Lamy, D. Perceptual Processing is Not Spared During the Attentional Blink. *J Cogn* **1**, 18 (2018).
15. Vogel, E. K., Luck, S. J. & Shapiro, K. L. Electrophysiological evidence for a postperceptual locus of suppression during the attentional blink. *J Exp Psychol Hum Percept Perform* **24**, 1656–1674 (1998).
16. Nieuwenstein, M. R., Chun, M. M., van der Lubbe, R. H. J. & Hooge, I. T. C. Delayed Attentional Engagement in the Attentional Blink. *J Exp Psychol Hum Percept Perform* **31**, 1463–1475 (2005).
17. Jolicœur, P. & Dell'Acqua, R. The Demonstration of Short-Term Consolidation. *Cogn Psychol* **36**, 138–202 (1998).
18. Dell'Acqua, R., Sessa, P., Jolicœur, P. & Robitaille, N. Spatial attention freezes during the attention blink. *Psychophysiology* **43**, 394–400 (2006).
19. Luck, S. J., Vogel, E. K. & Shapiro, K. L. Word meanings can be accessed but not reported during the attentional blink. *Nature* **383**, 616–618 (1996).
20. Sergent, C., Baillet, S. & Dehaene, S. Timing of the brain events underlying access to consciousness during the attentional blink. *Nat Neurosci* **8**, 1391–400 (2005).

21. Vogel, E. K. & Luck, S. J. Delayed working memory consolidation during the attentional blink. *Psychon Bull Rev* **9**, 739–743 (2002).
22. Lasaponara, S., Dragone, A., Lecce, F., Di Russo, F. & Doricchi, F. The “serendipitous brain”: Low expectancy and timing uncertainty of conscious events improve awareness of unconscious ones (evidence from the Attentional Blink). *Cortex* **71**, 15–33 (2015).
23. Kranczioch, C., Debener, S. & Engel, A. K. Event-related potential correlates of the attentional blink phenomenon. *Cognitive Brain Research* **17**, 177–187 (2003).
24. Kranczioch, C., Debener, S., Maye, A. & Engel, A. K. Temporal dynamics of access to consciousness in the attentional blink. *Neuroimage* **37**, 947–955 (2007).
25. Marois, R., Chun, M. M. & Gore, J. C. Neural Correlates of the Attentional Blink. *Neuron* **28**, 299–308 (2000).
26. Cooper, A. C. G., Humphreys, G. W., Hulleman, J., Praamstra, P. & Georgeson, M. Transcranial magnetic stimulation to right parietal cortex modifies the attentional blink. *Exp Brain Res* **155**, 24–29 (2004).
27. Kihara, K. *et al.* The role of left and right intraparietal sulcus in the attentional blink: a transcranial magnetic stimulation study. *Exp Brain Res* **178**, 135–140 (2007).
28. Williams, M. A., Visser, T. A. W., Cunnington, R. & Mattingley, J. B. Attenuation of Neural Responses in Primary Visual Cortex during the Attentional Blink. *The Journal of Neuroscience* **28**, 9890–9894 (2008).
29. Gross, J. *et al.* Modulation of long-range neural synchrony reflects temporal limitations of visual attention in humans. *Proceedings of the National Academy of Sciences* **101**, 13050–13055 (2004).
30. Green, D. M. , & Swets, J. A. *Signal Detection Theory and Psychophysics.* (1966).
31. Luo, T. Z. & Maunsell, J. H. R. Neuronal Modulations in Visual Cortex Are Associated with Only One of Multiple Components of Attention. *Neuron* **86**, 1182–8 (2015).
32. Sridharan, D., Steinmetz, N. A., Moore, T. & Knudsen, E. I. Does the Superior Colliculus Control Perceptual Sensitivity or Choice Bias during Attention? Evidence from a Multialternative Decision Framework. *The Journal of Neuroscience* **37**, 480–511 (2017).
33. Caetta Florent, G. A. Upshifted decision criteria in attentional blink and repetition blindness. *Visual Cognition* **18**, 413–433 (2010).
34. Macmillan, N. A. & Creelman, C. D. *Detection Theory*. (Psychology Press, 2004). doi:10.4324/9781410611147.
35. DeCarlo, L. T. On a signal detection approach to -alternative forced choice with bias, with maximum likelihood and Bayesian approaches to estimation. *J Math Psychol* **56**, 196–207 (2012).
36. Sridharan, D., Steinmetz, N. A., Moore, T. & Knudsen, E. I. Distinguishing bias from sensitivity effects in multialternative detection tasks. *J Vis* **14**, 16–16 (2014).
37. Parker, A. J. & Newsome, W. T. SENSE AND THE SINGLE NEURON: Probing the Physiology of Perception. *Annu Rev Neurosci* **21**, 227–277 (1998).
38. Funahashi, S. Working Memory in the Prefrontal Cortex. *Brain Sci* **7**, 49 (2017).
39. Zhang, Y., Bi, K., Li, J., Wang, Y. & Fang, F. Dyadic visual perceptual learning on orientation discrimination. *Current Biology* **33**, 2407-2416.e4 (2023).
40. Dupont, P. *et al.* Regions in the human brain activated by simultaneous orientation discrimination: a study with positron emission tomography. *European Journal of Neuroscience* **10**, 3689–3699 (1998).
41. Maunsell, J. H. R. Neuronal Mechanisms of Visual Attention. *Annu Rev Vis Sci* **1**, 373–391 (2015).

42. Sridharan, D., Steinmetz, N. A., Moore, T. & Knudsen, E. I. Distinguishing bias from sensitivity effects in multialternative detection tasks. *J Vis* **14**, 16–16 (2014).
43. Vrieze, S. I. Model selection and psychological theory: A discussion of the differences between the Akaike information criterion (AIC) and the Bayesian information criterion (BIC). *Psychol Methods* **17**, 228–243 (2012).
44. Akyürek, E. G., Leszczyński, M. & Schubö, A. The temporal locus of the interaction between working memory consolidation and the attentional blink. *Psychophysiology* no-no (2010) doi:10.1111/j.1469-8986.2010.01033.x.
45. Vogel, E. K., Luck, S. J. & Shapiro, K. L. Electrophysiological evidence for a postperceptual locus of suppression during the attentional blink. *J Exp Psychol Hum Percept Perform* **24**, 1656–1674 (1998).
46. Dell'Acqua, R., Sessa, P., Jolicœur, P. & Robitaille, N. Spatial attention freezes during the attention blink. *Psychophysiology* **43**, 394–400 (2006).
47. Jolicœur, P., Sessa, P., Dell'Acqua, R. & Robitaille, N. Attentional control and capture in the attentional blink paradigm: Evidence from human electrophysiology. *European Journal of Cognitive Psychology* **18**, 560–578 (2006).
48. Jolicœur, P., Sessa, P., Dell'Acqua, R. & Robitaille, N. On the control of visual spatial attention: evidence from human electrophysiology. *Psychol Res* **70**, 414–424 (2006).
49. Sheahan, H., Luyckx, F., Nelli, S., Teupe, C. & Summerfield, C. Neural state space alignment for magnitude generalization in humans and recurrent networks. *Neuron* **109**, 1214-1226.e8 (2021).
50. Chung, S. & Abbott, L. F. Neural population geometry: An approach for understanding biological and artificial neural networks. *Curr Opin Neurobiol* **70**, 137–144 (2021).
51. Correa, Á., Lupiáñez, J., Milliken, B. & Tudela, P. Endogenous temporal orienting of attention in detection and discrimination tasks. *Percept Psychophys* **66**, 264–278 (2004).
52. Lubbe, R. H. J. Van der, Vogel, R. O. & Postma, A. Different Effects of Exogenous Cues in a Visual Detection and Discrimination Task: Delayed Attention Withdrawal and/or Speeded Motor Inhibition? *J Cogn Neurosci* **17**, 1829–1840 (2005).
53. Treue, S. & Maunsell, J. H. R. Attentional modulation of visual motion processing in cortical areas MT and MST. *Nature* **382**, 539–541 (1996).
54. Luck, S. J. *et al.* Effects of spatial cuing on luminance detectability: Psychophysical and electrophysiological evidence for early selection. *J Exp Psychol Hum Percept Perform* **20**, 887–904 (1994).
55. McAdams, C. J. & Maunsell, J. H. R. Effects of Attention on Orientation-Tuning Functions of Single Neurons in Macaque Cortical Area V4. *The Journal of Neuroscience* **19**, 431–441 (1999).
56. Navalpakkam, V. & Itti, L. Search Goal Tunes Visual Features Optimally. *Neuron* **53**, 605–617 (2007).
57. Kanashiro, T., Ocker, G. K., Cohen, M. R. & Doiron, B. Attentional modulation of neuronal variability in circuit models of cortex. *Elife* **6**, (2017).
58. Averbeck, B. B., Latham, P. E. & Pouget, A. Neural correlations, population coding and computation. *Nat Rev Neurosci* **7**, 358–366 (2006).
59. Rotermund, D., Taylor, K., Ernst, U. A., Kreiter, A. K. & Pawelzik, K. R. Attention Improves Object Representation in Visual Cortical Field Potentials. *The Journal of Neuroscience* **29**, 10120–10130 (2009).
60. Zivony, A. & Lamy, D. What processes are disrupted during the attentional blink? An integrative review of event-related potential research. *Psychon Bull Rev* **29**, 394–414 (2022).

61. Akyürek, E. G., Leszczyński, M. & Schubö, A. The temporal locus of the interaction between working memory consolidation and the attentional blink. *Psychophysiology* no-no (2010) doi:10.1111/j.1469-8986.2010.01033.x.
62. Martens, S., Elmallah, K., London, R. & Johnson, A. Cuing and stimulus probability effects on the P3 and the AB. *Acta Psychol (Amst)* **123**, 204–218 (2006).
63. Jolicœur, P., Sessa, P., Dell'Acqua, R. & Robitaille, N. On the control of visual spatial attention: evidence from human electrophysiology. *Psychol Res* **70**, 414–424 (2006).
64. Reed, C. L. *et al.* Selective contributions of executive function ability to the P3. *International Journal of Psychophysiology* **176**, 54–61 (2022).
65. Freedman, D. J., Riesenhuber, M., Poggio, T. & Miller, E. K. Categorical Representation of Visual Stimuli in the Primate Prefrontal Cortex. *Science (1979)* **291**, 312–316 (2001).
66. Antzoulatos, E. G. & Miller, E. K. Synchronous beta rhythms of frontoparietal networks support only behaviorally relevant representations. *Elife* **5**, (2016).
67. Gross, J. *et al.* Modulation of long-range neural synchrony reflects temporal limitations of visual attention in humans. *Proceedings of the National Academy of Sciences* **101**, 13050–13055 (2004).
68. Murthy, V. N. & Fetz, E. E. Coherent 25- to 35-Hz oscillations in the sensorimotor cortex of awake behaving monkeys. *Proc Natl Acad Sci U S A* **89**, 5670–4 (1992).
69. Anton-Erxleben, K. & Carrasco, M. Attentional enhancement of spatial resolution: linking behavioural and neurophysiological evidence. *Nat Rev Neurosci* **14**, 188–200 (2013).
70. Fook K.Chua. The effect of target contrast on the attentional blink. *Percept Psychophys* **5**, 770–788 (2005).
71. Gold, J. I. & Shadlen, M. N. The neural basis of decision making. *Annu Rev Neurosci* **30**, 535–74 (2007).
72. M Kleiner, D. B. D. P. A. I. R. M. C. B. What's new in psychtoolbox-3. *Perception* **36**, 1–16 (2007).
73. Nakatani, C., Baijal, S. & van Leeeuwen, C. Curbing the attentional blink: Practice keeps the mind's eye open. *Neurocomputing* **84**, 13–22 (2012).
74. Junghofer, M., Elbert, T., Tucker, D. M. & Rockstroh, B. Statistical control of artifacts in dense array EEG/MEG studies. *Psychophysiology* **37**, 523–532 (2000).
75. Bokil, H., Andrews, P., Kulkarni, J. E., Mehta, S. & Mitra, P. P. Chronux: A platform for analyzing neural signals. *J Neurosci Methods* **192**, 146–151 (2010).
76. Mesulam, M.-M. Spatial attention and neglect: parietal, frontal and cingulate contributions to the mental representation and attentional targeting of salient extrapersonal events. *Philos Trans R Soc Lond B Biol Sci* **354**, 1325–1346 (1999).
77. Banerjee, S., Grover, S., Ganesh, S. & Sridharan, D. Sensory and decisional components of endogenous attention are dissociable. *J Neurophysiol* **122**, 1538–1554 (2019).
78. Sreenivasan, V. & Sridharan, D. Subcortical connectivity correlates selectively with attention's effects on spatial choice bias. *Proceedings of the National Academy of Sciences* **116**, 19711–19716 (2019).
79. Sagar, V., Sengupta, R. & Sridharan, D. Dissociable sensitivity and bias mechanisms mediate behavioral effects of exogenous attention. *Sci Rep* **9**, 12657 (2019).

# Figures and Legends

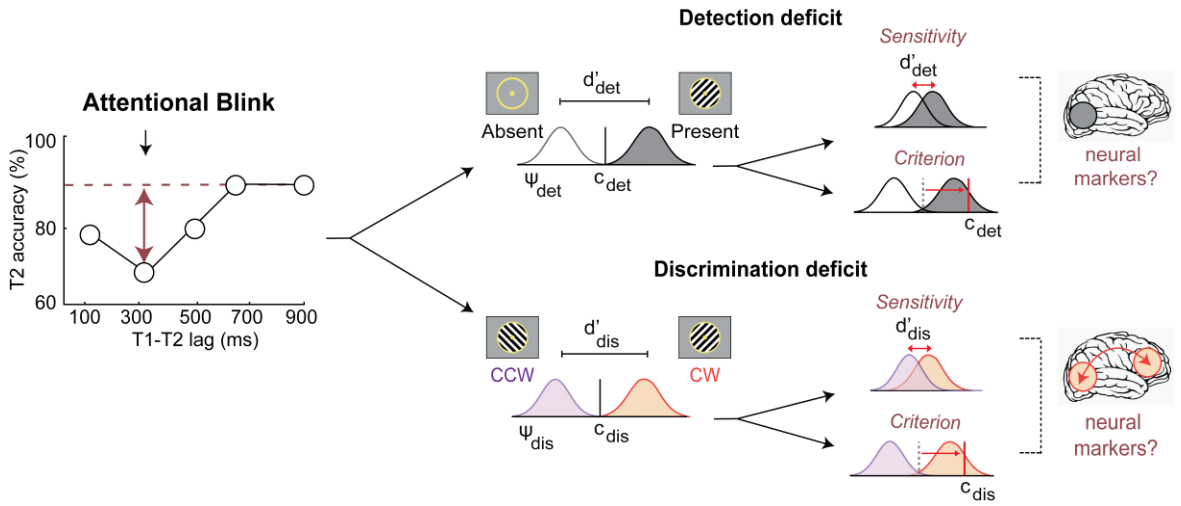


***Figure 1. Decoupling behavioral components and neural bases of the attentional blink.*** ***(Left)*** *Identifying the precise origin of accuracy deficits induced by the attentional blink. T2 identification accuracies at different inter-target (T1-T2) lags, in a conventional attentional blink task. x-axis: inter-target lag in milliseconds; y-axis: T2 identification accuracy (%). Red horizontal line: asymptotic T2 identification accuracy for long inter-target lags; red vertical arrows: accuracy deficit with T2 identification for short inter-target lags (attentional blink).* ***(Right, top)*** *The identification deficit could reflect impaired detection of T2's presence which, in turn, could arise either from a detection sensitivity deficit (upper row) or a detection bias (criterion) deficit (lower row). Gray and white Gaussians: decision variable distributions corresponding to signal (target present) and noise (target absent), respectively. Black vertical line: criterion for deciding between target present and absent.* ***(Right, bottom)*** *The identification deficit could also reflect impaired discrimination of T2's features (e.g. orientation), which, again, could arise either from a discrimination sensitivity deficit (upper row) or a discrimination bias (criterion) deficit (lower row). Purple and orange Gaussians: decision variable distributions corresponding to a counterclockwise (CW) and clockwise (CCW) gratings, respectively. Black vertical line: criterion for deciding between target features (clockwise and counterclockwise orientation).*

*Brain schematics (**rightmost column**): Distinct neural markers of each subcomponent – detection (top) or discrimination (bottom) -- of attentional blink deficits.*

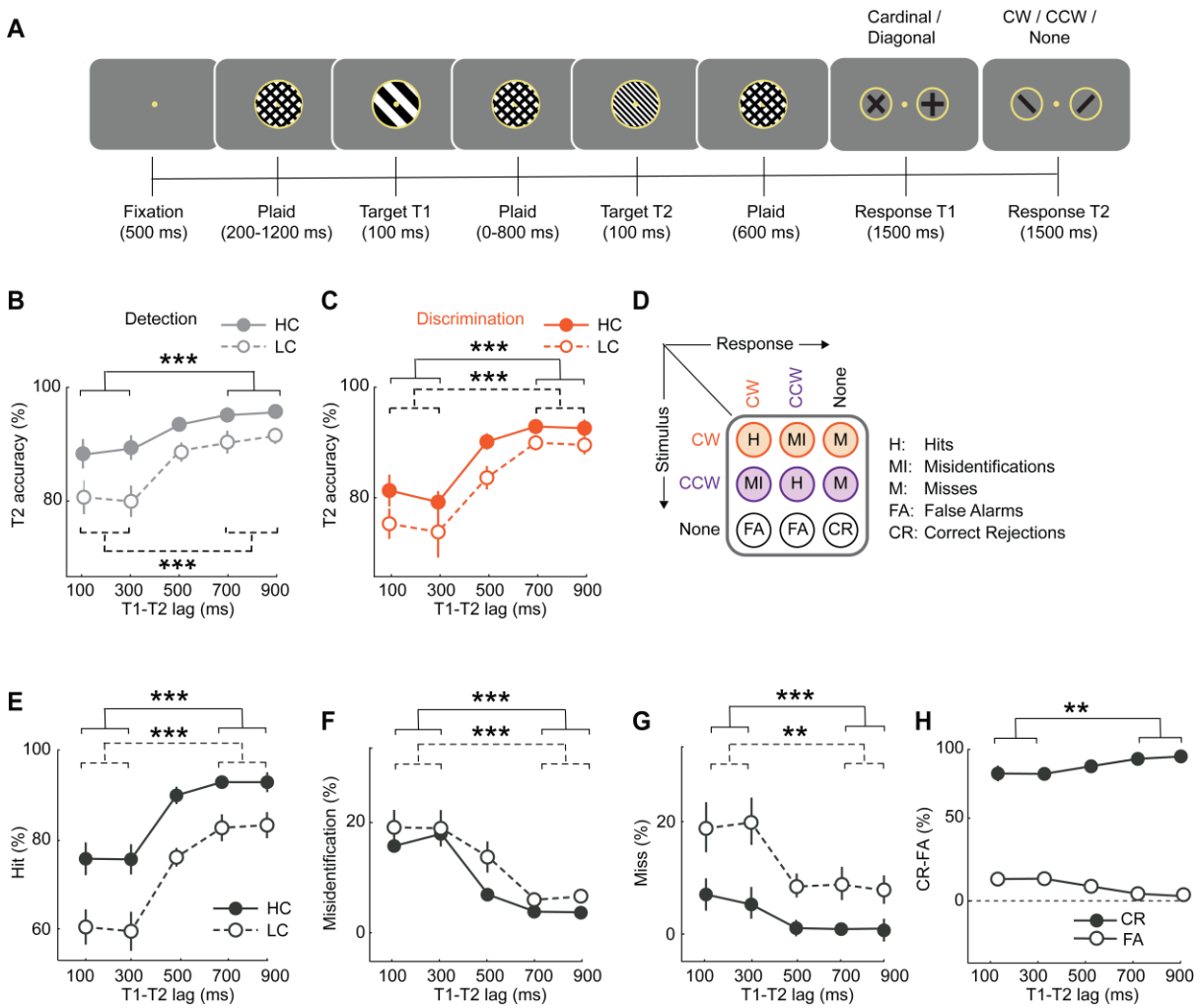


***Figure 2. Novel task design to distinguish subcomponents of the attentional blink.***

***A.*** *Schematic of the attentional blink task. Stimuli were presented in a rapid serial visual presentation (RSVP) paradigm at a 10 Hz rate (70 ms onset, 30 ms offset). Following fixation, plaid gratings appeared for a variable interval (200-1200 ms, geometrically distributed), followed by the first target (T1): a low spatial frequency grating (100 ms). After this a series of plaid gratings appeared for variable intervals (0, 200, 400, 600, and 800 ms; geometric distribution) followed by the appearance of the second target (T2): a high spatial frequency grating (100 ms). Following T2, plaid gratings were presented for a fixed interval (600 ms). Finally, in the response epoch, participants reported T1's orientation as*

*being closer to the cardinal or diagonal axes (two-alternative), and then reported T2's orientation as being clockwise or counterclockwise of vertical, or absent (three-alternative).*

***B.*** *Psychometric function of accuracy (% correct) for T2 detection with increasing inter target (T1-T2) lags, for trials in which T1 was reported correctly (n=24 participants). Filled circles and solid lines: average accuracy for high contrast T2 gratings; open circles and dashed lines: average accuracy for low contrast T2 gratings. Error bars: s.e.m. Asterisks: significance levels for comparing accuracies between short (100 and 300 ms) and long (700 and 900 ms) lag trials; solid and dashed brackets: comparisons for high and low contrast gratings respectively. *p<0.05, **p<0.01, ***p<0.001 and n.s.: not significant.*

***C.*** *Same as in panel B, but showing the psychometric function of accuracy for T2 discrimination with increasing inter target (T1-T2) lags (n=24). Other conventions are the same as in panel B, except that markers and lines are depicted in orange colour.*

***D.*** *Stimulus-response contingency table for the 3-alternative T2 decision. Rows represent the three possible T2 stimulus events: clockwise orientation (CW, orange), counterclockwise orientation (CCW, purple) or absent (none, gray). Columns represent three possible choices: clockwise (CW), counterclockwise (CCW) or absent (none). The table depicts the nine stimulus-response contingencies: two each of hit rates (H), misidentification rates (MI), miss rates (M), false alarm rates (FA) – one for each orientation (CW/CCW) – and one correct rejection rate (CR).*

***E.*** *Same as in panel B, but showing psychometric function of average hit rates.*

***F.*** *Same as in panel B, but showing psychometric function of average misidentification rates.*

***G.*** *Same as in panel B, but showing psychometric function of average miss rates.* ***(E-G).*** *Other conventions are the same as in panel B except that markers and lines are denoted in black color.*

***H.*** *Same as in panel B, but showing psychometric function correct rejection (filled circles) and false alarm (open circles) rates on T2 absent trials.*

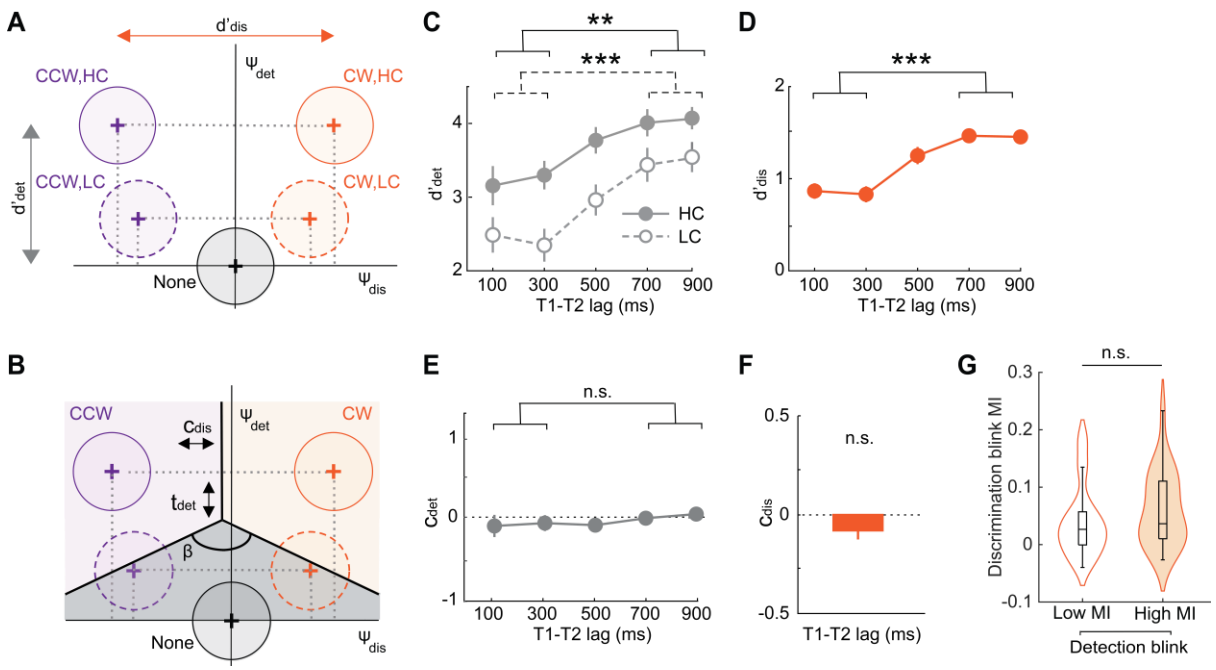


***Figure 3. A novel psychophysical model decouples attentional blink subcomponents.***

***A.*** *Signal detection model for estimating T2 sensitivity and bias. The decision variable is a bivariate Gaussian (**Ψ**) whose components, $\Psi_{det}$ (ordinate) and $\Psi_{dis}$ (abscissa), encode sensory evidence for stimulus presence and orientation, respectively. Black circle: **Ψ** distribution for T2 absent trials (noise distribution), is centered on the origin. Orange and purple circles: **Ψ** distributions for clockwise and counterclockwise T2 orientations, respectively (signal distributions). Solid and dashed outlines: High and low contrast T2, respectively. Vertical gray and horizontal orange lines (double headed arrows): detection sensitivity ($d'_{det}$) and discrimination sensitivity ($d'_{dis}$) for high contrast T2, respectively. Dashed gray lines: Signal mean projections onto the detection and discrimination axes.*

***B.*** *Decision surface with linear decision boundaries (thick black lines) demarcates 3 decision zones, one for each potential 3AFC choice: Clockwise T2 (CW, orange shading), counterclockwise T2 (CCW, purple shading), no T2 (None, gray shading). The decision surface is parameterized by: i) a discrimination criterion ($c_{dis}$), governing the horizontal position of the decision surface (horizontal double arrowhead), ii) a detection threshold ($t_{det}$), governing the vertical position of the decision surface (vertical double arrowhead),*

*and iii) the angle between the two oblique decision boundaries ($\beta$). Other conventions are the same as in panel A.*

***C.*** *Psychophysical function of detection sensitivity ($d'_{det}$) with increasing inter target (T1-T2) lags. Other conventions are the same as in Figure 2A.*

***D.*** *Same as in panel C but showing the psychophysical function of discrimination sensitivity ($d'_{det}$). Model selection yielded identical psychophysical functions for high and low contrast T2 (Methods). Other conventions are the same as in Figure 2B.*

***E.*** *Same as in panel C but showing the psychophysical function of detection criterion ($c_{det}$). Dashed horizontal line: $c_{det}=0$.*

***F.*** *Discrimination criterion ($c_{dis}$). Model selection constrained $c_{dis}$ to be equal across lags (Methods). Other conventions are the same as in panels D-E.*

***G.*** *Modulation index (MI) of the discrimination blink for low (open plot) and high (filled plot) detection blink MI blocks. Box plots, center line: median; box limits: upper and lower quartiles; whiskers: 1.5x the interquartile range. Violin plots: kernel density estimates.*

*(C-G) Asterisks: *p<0.05, **p<0.01, ***p<0.001; and n.s.: not significant.*

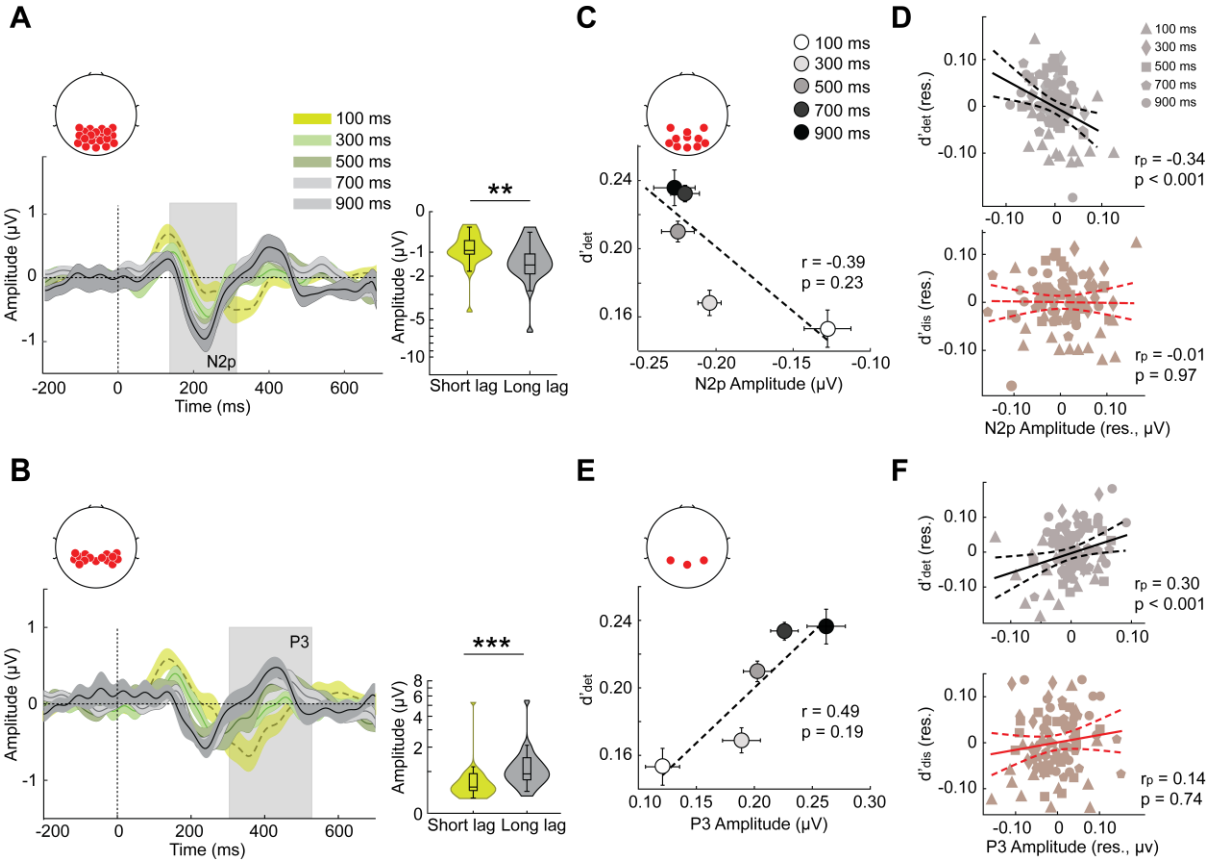


***Figure 4. N2p and P3 event related potentials signal detection sensitivity deficits.***

***A.*** *(Left) The event related potential (ERP, n=18 participants) showing the N2p component in occipitoparietal electrodes (inset), locked to T2 onset (dashed vertical line). Bright green, dull green, dark green, light gray and black traces: Average ERPs for the five inter-target lags – 100, 300, 500, 700 and 900 ms – respectively. Shading: s.e.m. Gray vertical shading: Time epoch for N2p amplitude quantification. ERPs were computed by subtracting the average ERPs on correct rejection trials (Methods). (Right) Violin plots showing the distribution of the peak N2p amplitudes across participants separately for the short (green: 100+300 ms) and the long (gray: 700+900 ms) lag trials. Asterisks: *p<0.05, **p<0.01, and ***p<0.001. Other conventions are the same as in Figure 3G.*

***B.*** *(Left) Same as in panel A (left) but showing the P3 ERP component in the parietal electrodes (inset). (Right) Same as in panel A (left) but showing the quantification of the P3 ERP. Other conventions are the same as in panel A.*

***C.*** *Variation of detection sensitivity ($d'_{det}$; y-axis) with N2p peak amplitude (x-axis) across inter-target lags (circles). r and p denote the robust correlation coefficient and permutation test p-value, respectively (Methods). Dashed line: linear fit. Error bars: s.e.m.*

***D.*** *(Top) Partial correlation between N2p peak amplitude (x-axis, amplitude residual) and detection sensitivity (y-axis, $d'_{det}$ residual) while controlling for the discrimination sensitivity ($d'_{dis}$). Each of the five shapes – filled triangle, diamond, square, pentagon, circle – represents one inter-target lag (legend). $r_p$ and p denote the partial correlation coefficient and permutation test p-value, respectively (Methods). Solid line: Linear fit; dashed curves: 95% confidence intervals. (Bottom) Same as in the top panel but showing partial correlation between N2p peak amplitude (x-axis, amplitude residual) and discrimination sensitivity (y-axis, $d'_{dis}$ residual) while controlling for detection sensitivity ($d'_{det}$).*

***E.*** *Same as in panel C but showing variation of discrimination sensitivity ($d'_{dis}$, y-axis) with P3 peak amplitude (x-axis) across inter-target lags.*

***F.*** *Same as in panel D but showing the partial correlation of P3 peak amplitude with $d'_{det}$ while controlling for $d'_{dis}$ (top), or, conversely, with $d'_{dis}$ while controlling for $d'_{det}$ (bottom).*

*(E-F) Other conventions are the same as in panels C-D, respectively.*

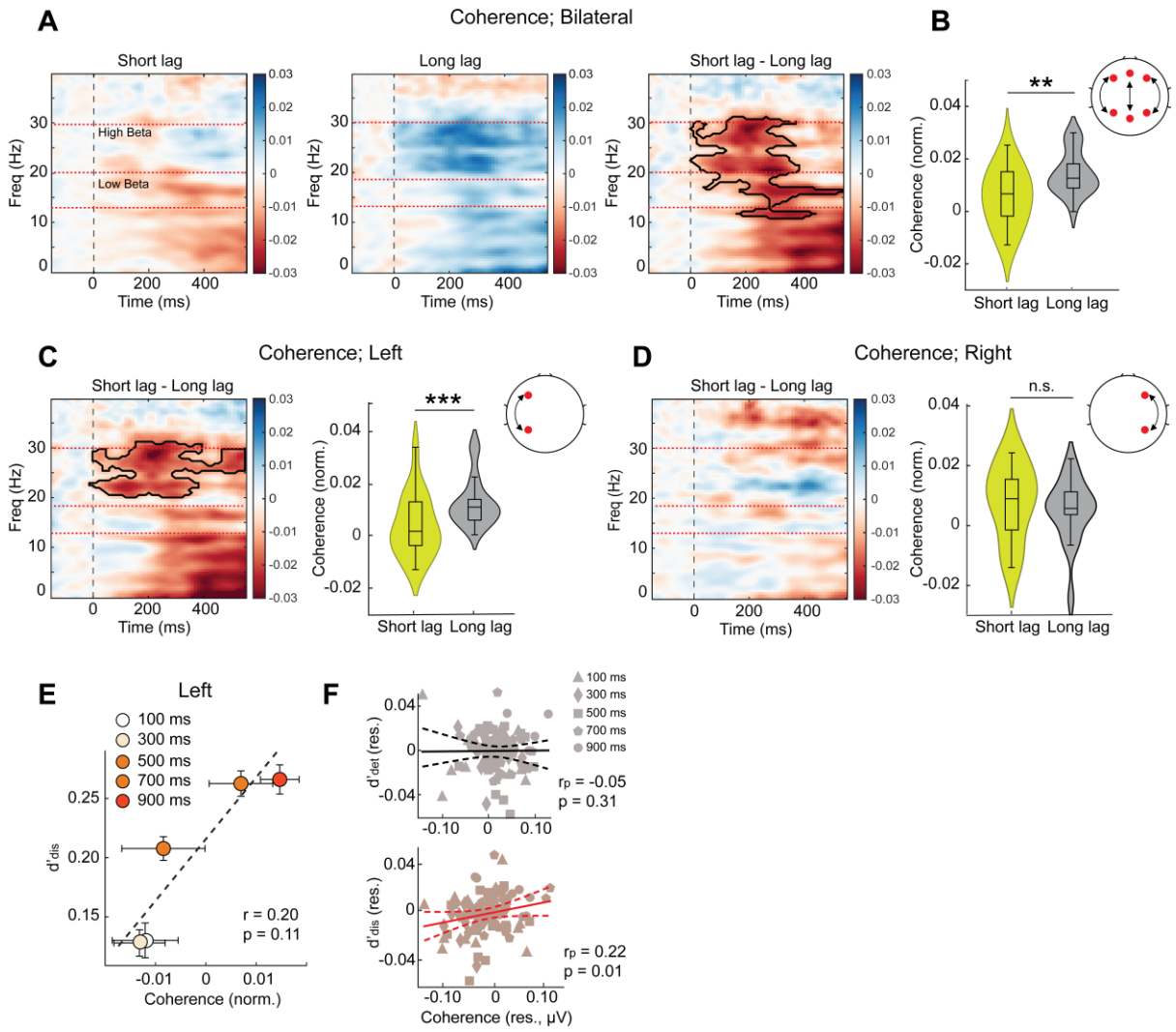


***Figure 5. High-beta fronto-parietal coherence signals discrimination sensitivity deficits.***

***A.*** *Coherence between frontal and parietal electrodes (Methods) as a function of time (x-axis) and frequency (y-axis) locked to T2 onset (t=0) (n=18 participants), normalized frequency-wise by a baseline mean (gray horizontal bar), and computed by subtracting the average coherograms for correct rejection trials. Cooler colors: higher coherence. Dashed horizontal line: low-beta (13 to 19 Hz) and high-beta (20 to 30 Hz) sub-bands. (Left and middle) Coherograms for the short (100+300 ms) and long (700+900 ms) lag trials, respectively. (Right) Difference coherogram. Bold black outline: statistically significant coherence difference between short and long lag trials (cluster forming threshold p<0.05).*

***B.*** *Bilateral fronto-parietal coherence values in the high-beta band across participants, separately for the short (100+300 ms, green) and long (700+900 ms, gray) lag trials. Topoplot: schematic of electrode pairs (red circles and black arrows) used for computing bilateral frontoparietal coherence (Methods). Other conventions are the same as in Figure 3G.*

***C.*** *(Left) Same as in panel A (right panel) but showing the difference coherogram for the left hemispheric frontoparietal electrodes. Other conventions are the same as in panel A. (Right) Same as in panel B but showing high-beta coherence values over the left hemispheric fronto-parietal electrodes. Other conventions are the same as in panel B and Figure 3G.*

***D.*** *(Left and right) Same as in panel C but showing the difference coherogram for the right hemispheric fronto-parietal electrodes. Other conventions are the same as in panel C. (B-D). Asterisks: *p<0.05, **p<0.01, and ***p<0.001.*

***E.*** *Same as Figure 4E but showing the variation of discrimination sensitivity ($d'_{dis}$, y-axis) with left fronto-parietal high-beta coherence (x-axis) across inter-target lags. Other conventions are the same as in Figure 4E.*

***F.*** *Same as in Figure 4F but showing the partial correlation of high-beta left fronto-parietal coherence with $d'_{det}$ while controlling for $d'_{dis}$ (top), or, conversely, with $d'_{dis}$ while controlling for $d'_{det}$ (bottom). Other conventions are the same as in Figure 4F.*

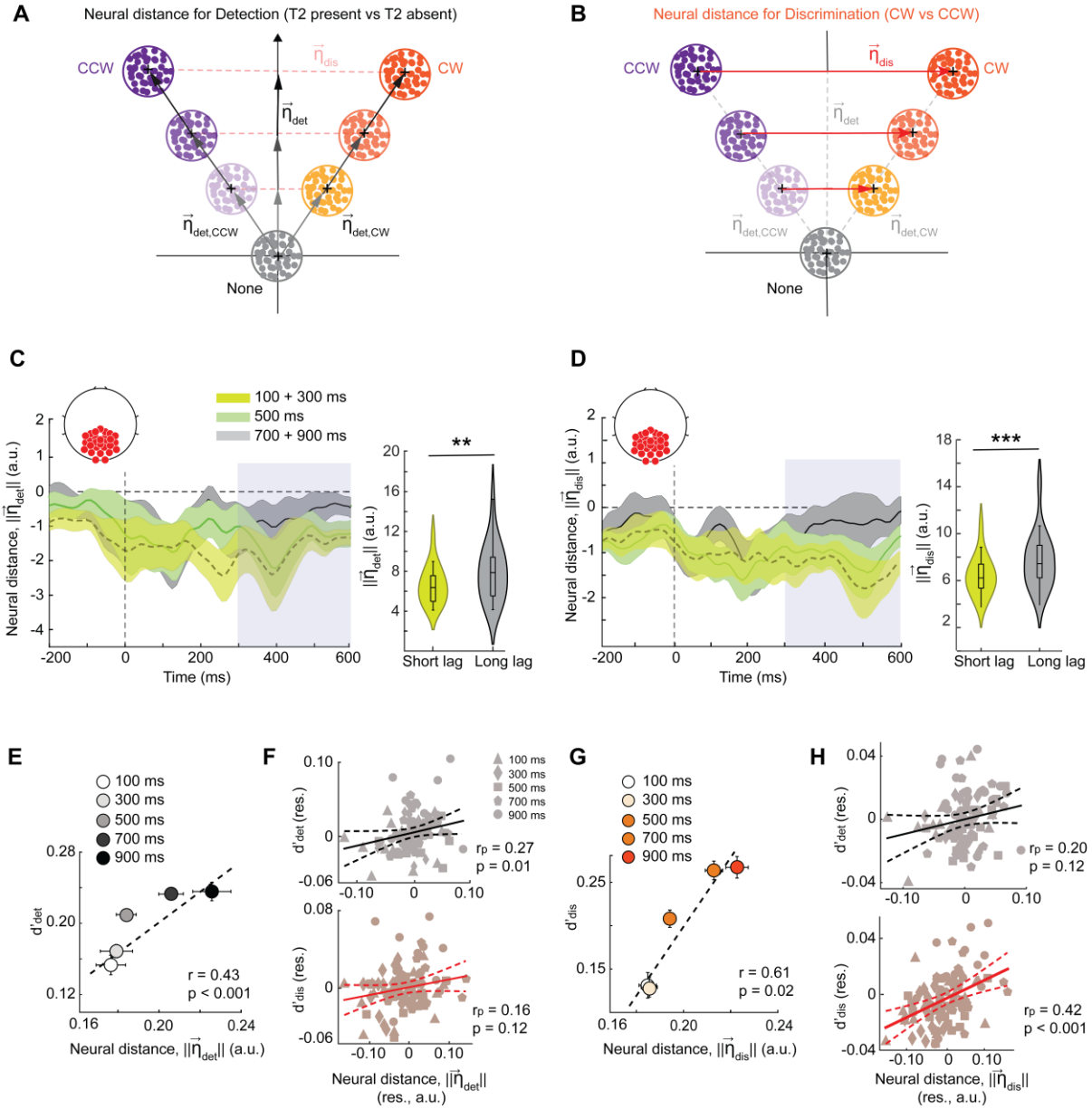


***Figure 6. Distinct neural dimensions encode détection and discrimination bottlenecks.***

***A.*** *Schematic showing the "detection" dimension, $\eta_{det}$ (y-axis): a linear dimension in a multidimensional electrode space along which neural activity encodes the presence versus absence of T2 (Methods). Gray, orange and purple dot clusters: distribution of EEG activity for T2 absent, T2 clockwise (CW) and counterclockwise (CCW) trials, respectively. Darker (lighter) shades denote longer (shorter) inter-target lags.*

***B.*** *Same as in panel A but showing the "discrimination" dimension, $\eta_{dis}$ (x-axis): a linear dimension along which neural activity encodes the orientation of T2 (clockwise versus counterclockwise of vertical).*

***C.*** *(Left) Time evolution of the average inter-class distance along the detection dimension ($||\eta_{det}||$) locked to T2 onset (n=18 participants). Values at each time point are plotted relative to the longest lag (900 ms). Bright green, dark green and black traces: short (100+300 ms) intermediate (500 ms) and long (700 ms) lags, respectively. Shading: s.e.m. Dashed vertical line: T2 onset. Gray shading: Time epoch for neural distance quantification and statistical comparison. (Right) Distribution of $\eta_{det}$ inter-class distances across participants separately for the short (green, 100+300 ms) and the long (gray, 700+900 ms) lag trials. Asterisks: *p<0.05, **p<0.01, and ***p<0.001. Other conventions are the same as in Figure 3G.*

***D.*** *Same as in panel C but showing the time evolution of the average neural inter-class distance along the discrimination dimension ($||\eta_{dis}||$) (left), and the distribution of neural distances along the discrimination dimension (right). Other conventions are the same as in panel C.*

***E.*** *Same as in Figure 4C, but showing variation of detection sensitivity ($d'_{det}$, y-axis) with neural distance along the detection dimension ($||\eta_{det}||$, x-axis) across inter-target lags.*

***F.*** *Same as in Figure 4D but showing the partial correlation of $||\eta_{det}||$ with $d'_{det}$ while controlling for $d'_{dis}$ (top), or, conversely, with $d'_{dis}$ while controlling for $d'_{det}$ (bottom).*

***G.*** *Same as in Figure 4E, but showing variation of discrimination sensitivity ($d'_{dis}$, y-axis) with neural distance along the discrimination dimension ($||\eta_{dis}||$, x-axis) across inter-target lags.*

***H.*** *Same as in Figure 4F but showing the partial correlation of $||\eta_{dis}||$ with $d'_{det}$ while controlling for $d'_{dis}$ (top), or, conversely, with $d'_{dis}$ while controlling for $d'_{det}$ (bottom).*

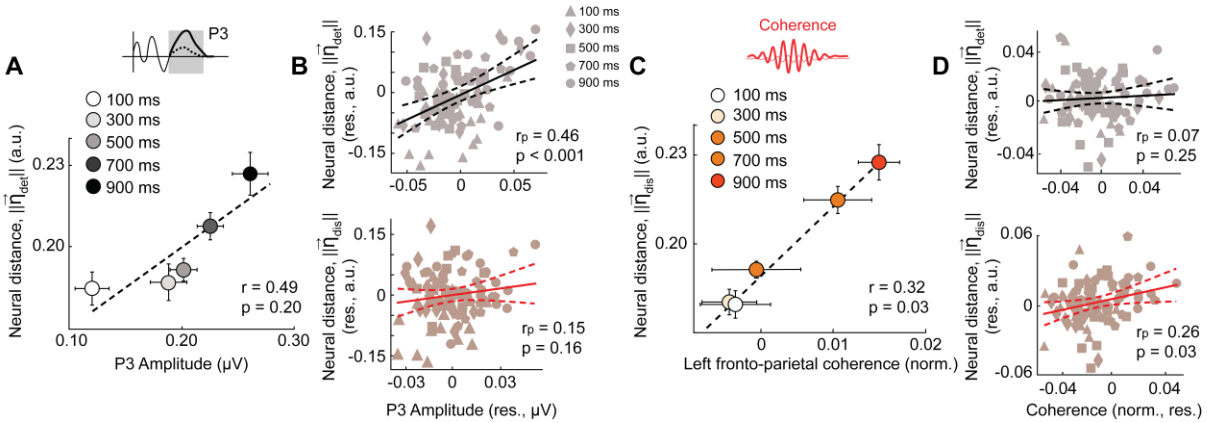


***Figure 7. Neural dimensions of detection and discrimination deficits correlate with their respective EEG markers.***

***A.*** *Same as in Figure 4C, but showing variation of the neural distance along the detection dimension ($||\eta_{det}||$, y-axis) with P3 amplitude ($d'_{det}$, x-axis) across inter-target lags.*

***B.*** *Same as in Figure 4D but showing the partial correlation of the P3 amplitude with $||\eta_{det}||$ while controlling for $||\eta_{dis}||$ (top), or, conversely, with $||\eta_{dis}||$ while controlling for $||\eta_{det}||$ (bottom).*

*(A-B) Other conventions are the same as in Figures 4C-D.*

***C.*** *Same as in Figure 4E, but showing variation of the neural distance along the discrimination dimension ($||\eta_{dis}||$, y-axis) with left high beta frontoparietal coherence (x-axis) across the 5 inter-target lags.*

***D.*** *Same as in Figure 4F but showing the partial correlation of the left high beta frontoparietal coherence with $||\eta_{det}||$ while controlling for $||\eta_{dis}||$ (top), or, conversely, with $||\eta_{dis}||$ while controlling for $||\eta_{det}||$ (bottom).*

*(C-D) Other conventions are the same as in Figures 4E-F.*

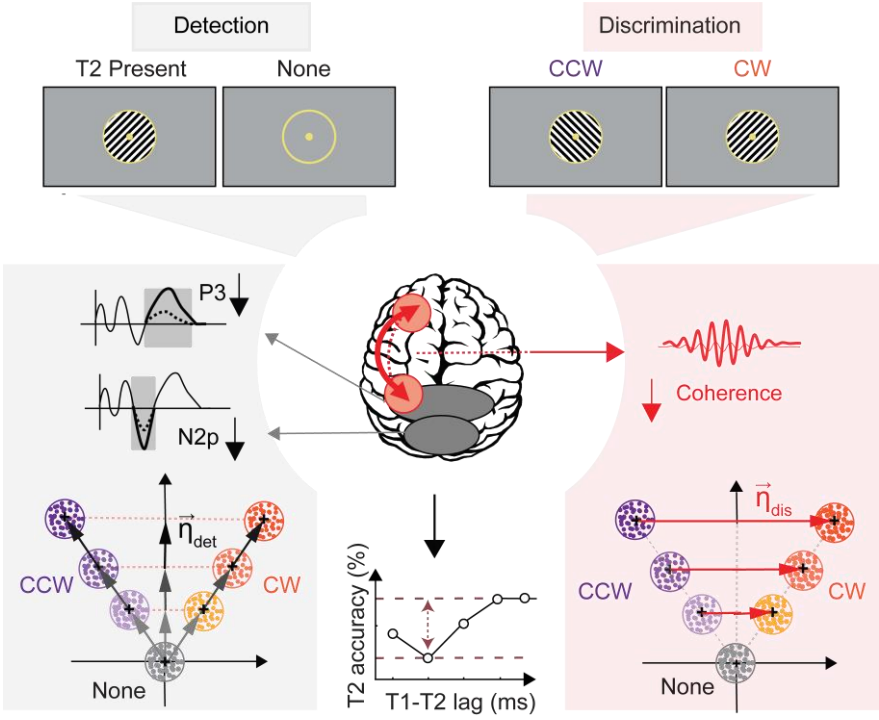


***Figure 8: Distinct neural bases of subcomponents of the attentional blink***

*The attentional blink selectively impairs a specific component of attention – perceptual sensitivity (d') – and produces both detection (top, left) and discrimination (top, right) deficits. Detection d' deficits – deficits with distinguishing the presence versus absence of the second target (T2) – are correlated with reduced amplitudes of N2p and P3 ERPs (gray shading, left top). They are also accompanied by a representational collapse along the detection dimension (gray shading, left bottom). By contrast, discrimination d' deficits – deficits with discriminating T2's orientation – are evidenced by reduced left fronto-parietal beta coherence (red shading, left top) and a representational collapse along the discrimination dimension (red shading, left bottom).*

# Supplementary Figures and Tables

**A**

| Model # | # Model parameters | Constraints |
|---|---|---|
| Model I | 35 | No constraints |
| Model II | 31 | Constant beta (lags) |
| Model III | 22 | Constant beta (lags),<br>Constant $c_{dis}$ (lags and contrast),<br>Constant $d'_{dis}$ (contrast) |
| Model IV | 22 | Constant beta (lags),<br>Constant $c_{det}$ (lags and contrast),<br>Constant $d'_{det}$ (contrast) |
| Model V | 13 | Constant beta (lags),<br>Constant $c_{det}$ (lags and contrast),<br>Constant $d'_{det}$ (contrast)<br>Constant $c_{dis}$ (lags and contrast),<br>Constant $d'_{dis}$ (contrast) |

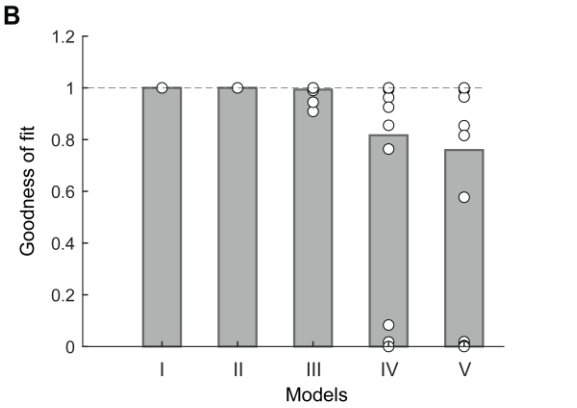


**C**

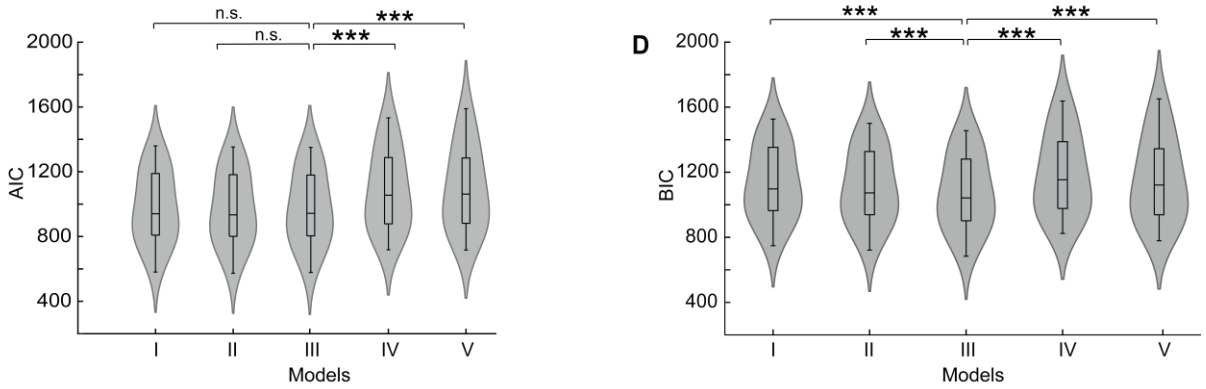


**Supplementary Figure S1. Model comparison analysis.**

**A.** Summary of the 5 models used in the analysis (see Methods for details).

**B.** Distribution of goodness of fit (p-values) with a randomization test based on the chi-squared statistic for all five models (model I – V, n=24 participants). Other conventions for the violin plot same as in Figure 3G (main text).

**C.** Distribution of Akaike information criterion (AIC) values for all five models. Other conventions are the same as in panel B.

**D.** Same as panel C but showing the distribution of Bayesian information criterion (BIC) values for all five models. Other conventions are the same as in panel C.

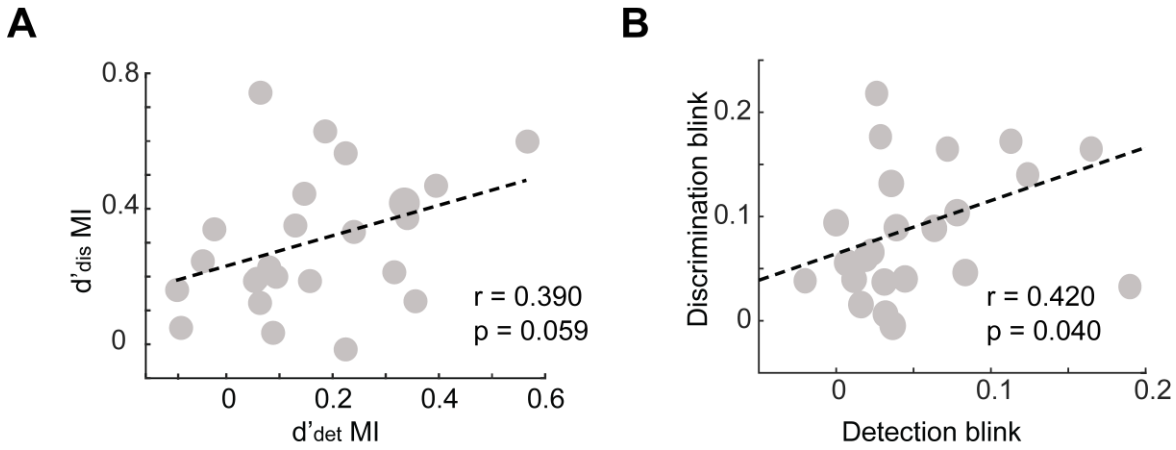


**Supplementary Figure S2. Correlation between detection and discrimination blink.**

**A.** Correlation between the modulation indices (MI) of detection and discrimination sensitivity. The MI is calculated as MI-$d'_{det}$ = ($d'_{det}^{LL}$ - $d'_{det}^{SL}$)/ ($d'_{det}^{LL}$ + $d'_{det}^{SL}$) (SL: short lag, LL: long lag; Methods)**.** Gray circles: individual participants. Dashed line: Linear fit. r and p values: correlation coefficient and its significance level based on robust correlations (Methods).

**B.** Same as in panel A except showing the correlation between MIs for detection and discrimination accuracy. Other conventions are the same as in panel A.

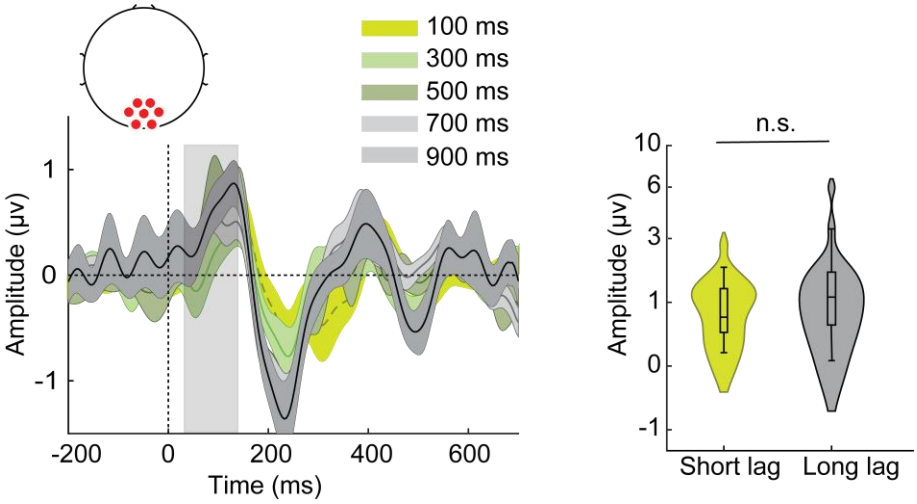


**Supplementary Figure S3. P1 ERP component in occipital electrodes.**

(Left) The P1 event related potential (ERP) in the bilateral occipital electrodes (inset, topoplot), locked to T2 grating onset (n=18 participants). Bright green, dull green, dark green, light gray and black traces: Average ERPs for the five inter-target lags (100, 300, 500, 700 and 900 ms), respectively. Shading: s.e.m. Gray vertical bar: Time epoch considered for quantifying the P1 component amplitude. Dashed vertical black line: T2 onset. Here, and elsewhere, ERPs were computed by subtracting the average ERPs for correct rejection trials (Methods). (Right) Violin plots showing the distribution of the peak P1 amplitudes across participants separately for the short (green; 100+300 ms) and the long (gray, 700+900 ms) lag conditions. Asterisks denote significance differences: *p<0.05, **p<0.01, and ***p<0.001. Other conventions for the violin plot are the same as in Figure 3G.

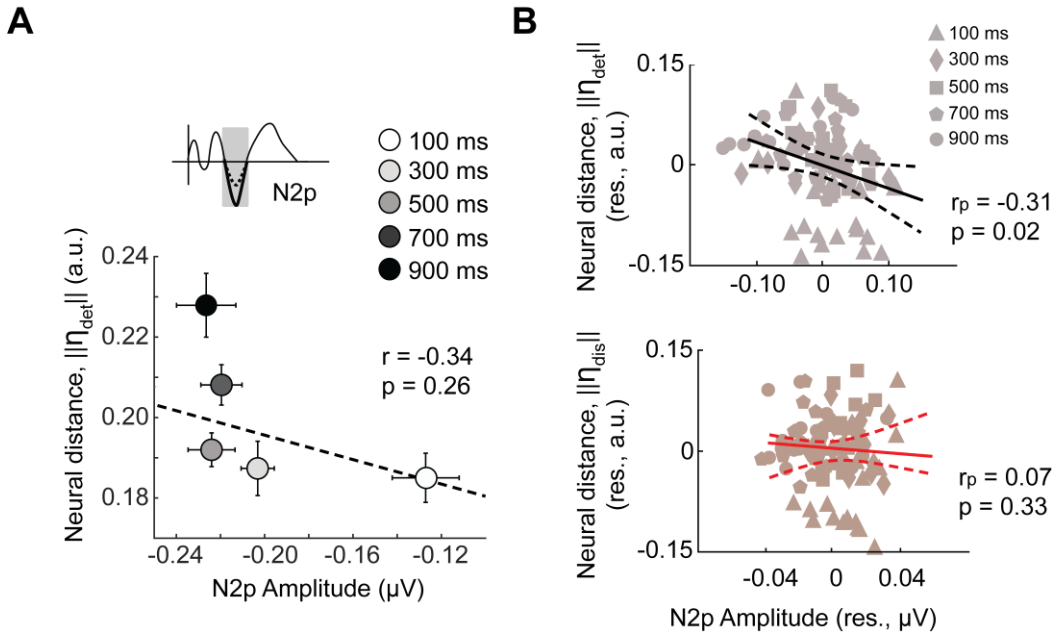


**Supplementary Figure S4. Linking neural dimensions with neural markers of detection deficits – N2p peak amplitude.**

**A.** Variation of the neural distance along the detection dimension ($||\eta_{det}||$, y-axis) with N2p amplitude ($d'_{det}$, x-axis) across the 5 inter-target lags (circles in distinct shades of gray). Dashed curve: linear fit. Error bars: s.e.m along the respective axis.

**B.** (Top) Partial correlation of the N2p peak amplitude (x-axis, amplitude residual) with $||\eta_{det}||$ (y-axis, detection distance residual) while controlling for $||\eta_{dis}||$. The five shapes – filled triangle, diamond, square, pentagon, circle – represent the five inter-target lags – 100, 300, 500, 700 and 900 ms – respectively (data pooled across n=18 participants). $r_p$ and p denote the partial correlation value and p-value calculated with a permutation test (Methods). Solid line: Linear fit; black dashed curves: 95% confidence intervals. (Bottom) Same as in the top panel but showing the partial correlation between N2p peak amplitude (x-axis, amplitude residual) with $||\eta_{dis}||$ (y-axis, discrimination distance residual) while controlling for $||\eta_{det}||$. Other conventions are the same as in the top panel.

**Supplementary Table S1. Attentional blink effect on psychometric measures.**

2-way ANOVA analysis with the psychometric measures as dependent variables and lags and contrasts as independent factors.

| **Psychometric measures** | **Analysis of Variance (ANOVA)** | | |
|---|---|---|---|
| | Main effect of lag (F, p) | Main effect of contrast (F, p) | Interaction effect (F, p) |
| Hit | **40.94, <0.001** | **21.48, <0.001** | 0.41, 0.527 (n.s.) |
| Miss | **7.43, 0.011** | **11.35, 0.002** | 1.19, 0.285 (n.s) |
| Misidentification | **35.63, <0.001** | 2.39, 0.135 (n.s.) | 0.26, 0.618 (n.s) |
| FA | **10.3, 0.003** | N/A | N/A |
| CR | **10.3, 0.003** | N/A | N/A |

**Supplementary Table S2. Partial correlations of ERP amplitudes with detection and discrimination sensitivity.**

Magnitude of blink induced deficit in ERP amplitudes, and partial correlation between ERP amplitudes, and detection (discrimination) d', while controlling for the confounding effect of discrimination (detection) d' (Methods). **Bold** entries correspond to significant partial correlations.

| **ERP components** | **Blink deficit (mean ± s.e.m)** | **Partial correlation with sensitivity (d')** | |
|---|---|---|---|
| | | Partial correlation with detection d' | Partial correlation with discrimination d' |
| P1 (occipital) | 0.24 ± 0.11, p = 0.050 | $r_p$ = 0.14 p = 0.575 | $r_p$ = -0.02 p = 0.999 |
| P2 (frontocentral) | 0.19 ± 0.07, p = 0.021 | $r_p$ = 0.05 p = 0.999 | $r_p$ = 0.23 p = 0.120 |
| N2p (occipitoparietal) | **-0.47 ± 0.12, p = 0.003** | **$r_p$ = -0.34 p < 0.001** | $r_p$ = -0.01 p = 0.970 |
| P3 (parietal) | **0.45 ± 0.09, p < 0.001** | **$r_p$ = 0.30 p < 0.001** | $r_p$ = 0.14 p = 0.748 |

**Supplementary Table S3. Partial correlation of fronto-parietal coherence with detection and discrimination sensitivity.**

Partial correlation between left and right frontoparietal beta coherence and detection and discrimination sensitivity. Other conventions are the same as in SI Table S2.

| **Hemisphere** | **Beta band** | **Partial correlation with sensitivity (d')** | |
|---|---|---|---|
| | | Partial correlation with detection d' | Partial correlation with discrimination d' |
| Left fronto-parietal | High beta (20-30 Hz) | $r_p$ = -0.05<br>p = 0.316 | **$r_p$ = 0.22**<br>**p = 0.018** |
| | Low beta (13-19 Hz) | $r_p$ = 0.05<br>p = 0.728 | $r_p$ = -0.03<br>p = 0.728 |
| Right fronto-parietal | High beta (20-30 Hz) | $r_p$ = -0.01<br>p = 0.470 | $r_p$ = 0.21<br>p = 0.1 |
| | Low beta (13-19 Hz) | $r_p$ = -0.04<br>p = 0.680 | $r_p$ = 0.05<br>p = 0.682 |

**Supplementary Table S4. Partial correlation between neural measures and neural distances in the detection and discrimination dimensions.**

Partial correlation between neural measures (N2P and P3 ERP amplitudes and left frontoparietal high-beta coherence) and neural distances in detection (discrimination) dimension while controlling for the confounding effect of the neural distance in the discrimination (detection) dimension.

| **Neural measure** | **Partial correlation with neural distance ($\eta$)** | |
|---|---|---|
| | Neural distance in the detection dimension ($\|\|\eta_{det}\|\|$) | Neural distance in the discrimination dimension ($\|\|\eta_{dis}\|\|$) |
| N2p amplitude | **$r_p$ = -0.31, p = 0.02** | $r_p$ = 0.07, p = 0.330 |
| P3 amplitude | **$r_p$ = 0.46, p < 0.001** | $r_p$ = 0.15, p = 0.160 |
| Left fronto-parietal high-beta (20-30 Hz) coherence | $r_p$ = 0.07, p = 0.255 | **$r_p$ = 0.26, p = 0.039** |